Available online at www.sciencedirect.com
ScienceDirect
ELSEVIER
Palaeogeography, Palaeoclimatology, Palaeoecology 238 (2006) 399–423
PALAEO
www.elsevier.com/locate/palaeo

Reconstructing the Late Miocene climate and oceanic heat flux using the AGCM ECHAM4 coupled to a mixed-layer ocean model with adjusted flux correction

Anke Steppuhn, Arne Micheels *, Gunfried Geiger, Volker Mosbrugger

Institut für Geowissenschaften, Eberhard-Karls-Universität Tübingen, Sigwartstraße 10, D-72076 Tübingen, Germany

Received 29 June 2002; accepted 7 March 2006

Abstract

In terms of climate, the Late Miocene represents a transitional phase between the Eocene greenhouse climate and the Quaternary icehouse situation; it is characterised by an extensive Antarctic ice sheet and incipient glaciation in the Northern Hemisphere. In order to better understand the Late Miocene climate, we performed a simulation study for the Tortonian using the complex atmospheric general circulation model ECHAM4 coupled to a mixed-layer ocean model. The boundary conditions such as the orography and the continental ice distribution were adapted to the Tortonian conditions; considering the coarse geographic resolution of the model, the land–sea distribution was assumed to be similar to the present situation and the atmospheric CO_2 concentration was set to 353 ppm. Because the mixed-layer ocean model uses a flux correction tuned to the modern oceanic heat transport a method was developed to estimate the Tortonian palaeo-flux correction based on the zonally averaged SST gradients. As compared to the present-day world, the Tortonian model run shows a significant reduction in the oceanic heat transport, a considerable warming and reduction of sea ice in high latitudes, a weakening of the Asian monsoon, a cooling in the mid-latitudes–caused by the reduced oceanic heat transport–and an increase in precipitation in Southern Europe. Except for the cooling of the mid-latitudes these results are largely consistent with proxy-data and other modelling studies although the proxy data indicate much warmer conditions in high latitudes than calculated in the model. The reasons for the discrepancies between model-based and proxy data reconstructions are discussed.

Keywords: Climate modelling; Mixed-layer ocean model; Flux correction; Sea surface temperature; Miocene

1. Introduction

Recently, climate modelling has become an increasingly popular tool in palaeoclimate research (e.g. Dutton and Barron, 1996; Upchurch et al., 1999; Haywood et al., 2000; Sellwood et al., 2000): It has proved to be useful not only to reconstruct past climates and climate processes but also to validate climate models as well as empirical proxy data (e.g., Kutzbach et al., 1989; Sellwood et al., 2000). Within the framework of the EEDEN research program devoted to ecosystem and environment change in the Eurasian Neogene (see Agustí et al., 2006-this volume), we used this palaeoclimate modelling approach to analyse the basic global climate patterns and climate processes for selected Neogene time slices. As a first step, we focused on the Tortonian (Late Miocene, 11–7 Ma), a time

* Corresponding author. Fax: +49 7071 29 52 17.
E-mail address: arne.micheels@uni-tuebingen.de (A. Micheels).

0031-0182/$ - see front matter © 2006 Elsevier B.V. All rights reserved.
doi:10.1016/j.palaeo.2006.03.037

period characterised by intensive Antarctic glaciation and the beginning of glaciation in the North Atlantic region. Previous palaeoclimate research has primarily analysed typical greenhouse (e.g. Nikolaev et al., 1998; Upchurch et al., 1998; McGuffie et al., 1999; Upchurch et al., 1999) or icehouse situations (e.g. Herterich and Berger, 1993; Ganopolski et al., 1998a,b; Montoya et al., 1998; Kubatzki et al., 2000) whereas the intermediate climate system of the Miocene with a uni-polar glaciation has attracted relatively little interest so far (e.g. Dutton and Barron, 1997; Fluteau et al., 1999).

Palaeoclimate modelling can be done with several model concepts. One possibility is to run an atmospheric general circulation model (AGCM) to simulate the atmospheric processes only. An AGCM, however, requires a full description of the 'lower boundary conditions' including the sea surface temperatures (SST) of the palaeocean. Since the ocean covers about two third of the Earth's surface, a correct representation of the palaeo-SST distribution is essential to obtain realistic climate modelling results. Unfortunately, reliable SST information covering most of the ocean surface are difficult to obtain for pre-Quaternary time periods. To avoid the SST problem, fully coupled atmosphere–ocean general circulation models (AOGCM) can be used allowing for an independent calculation of the palaeo-SST. Yet, AOGCMs are very costly in terms of computing time and require detailed information about the palaeo-bathymetry of the ocean as well as about the continental freshwater runoff, both boundary conditions are again very difficult to obtain for pre-Quaternary situations. In between both strategies, the use of either AGCMs with prescription of SSTs or of fully coupled AOGCMs, there is a third possibility, i.e. to run an AGCM coupled to a simple mixed-layer ocean representing only the uppermost layer (about 50 m) of the ocean. These AGCM/ML models can also calculate the palaeo-SST independently but do not simulate the full oceanic circulation; the thermal effects of the ocean currents are only represented by a so-called flux correction which has to be adapted to the palaeo-situations.

In our modelling study on the Tortonian palaeoclimate, the AGCM/ML model concept is used. A new method on how the flux correction and, thus, the oceanic heat transport of the mixed-layer ocean can be adjusted to the palaeo-situation based on sparse δ^{18}O-data from planktonic foraminifera is proposed. Based on this method, the AGCM/ML model is run using the Tortonian palaeogeography, palaeorography and ice cover as lower boundary conditions. The model results clearly indicate a weaker poleward oceanic heat transport and a reduced mass transport into higher latitudes for the Tortonian. Despite this reduced oceanic heat transport, the globally averaged temperature for the Tortonian is almost identical to the recent value but the zonal pattern is significantly different from the present-day situation with a strong warming in the high northern latitudes. The overall Tortonian climate patterns and trends as calculated with the AGCM/ML model are largely consistent with existing proxy data although the modelled continental temperatures in the Northern Hemisphere are much too low. The reasons for the discrepancy between model and proxy data are discussed.

2. The model ECHAM4/ML and Tortonian boundary conditions

The atmospheric global circulation model (AGCM) used in this study was ECHAM4 (Roeckner et al., 1992; DKRZ Modellbetreuungsgruppe, 1994; Roeckner et al., 1996; DKRZ Modellbetreuungsgruppe, 1997) with a resolution of T30 corresponding to a spatial resolution of approximately 3.75°. The model is highly complex wherein dry dynamics are transformed with a spectral scheme and, for parameters such as the advection of water vapour, the semi-Lagrangian scheme is used. ECHAM4 includes (amongst others) processes related to radiation, cumulus convection, land surface, ice cover, etc. Improvements compared to the previous ECHAM3 (DKRZ Modellbetreuungsgruppe, 1994) concern, e.g. the parameterisations of the radiation and land surface processes. The ECHAM4 model represents the recent climatic state very well (e.g., Roeckner et al., 1996). Both, ECHAM4 and its previous version ECHAM3, have been used in numerous climate (e.g., Latif and Neelin, 1994) and palaeoclimate studies and have proved to be quite efficient in the palaeoclimate intercomparison project (PMIP, e.g. Lorenz et al., 1996).

In our study, the ECHAM model was coupled to a mixed-layer (ML) ocean model (further documentation is available from the DKRZ Modellbetreuungsgruppe). This mixed-layer ocean model includes ocean processes such as the heat transport in a more appropriate way than simply using SSTs. In this model, the heat budget of an oceanic mixed-layer with a constant depth of $h_0 = 50$ m is included:

$$C_0 \frac{\partial T_m}{\partial t} = H_a - \mathrm{div} T_0 \qquad (1)$$

where T_m, the temperature of the mixed-layer, is equivalent to the SST. C_0 describes the effective heat capacity of the oceanic mixed-layer and H_a represents the net heat flux at the sea surface while $\mathrm{div}T_0$ is the divergence of the oceanic heat transport. The

climatological average of this divergence term is also called the flux correction and is intended to compensate for the energy transport by ocean currents. The recent flux correction is reconstructed as to represent best the present-day heat exchange between atmosphere and ocean. It was calculated from different ECHAM4 runs with observed SSTs. Therein, the seasonal cycle is represented by monthly average values. As compared to oceanic general circulation models (OGCM), the advantage of the mixed-layer ocean model with its flux correction is the simple description of ocean properties. Neither a velocity field nor bathymetry of ocean basins or other parameters such as freshwater influxes have to be included.

Applying ECHAM4/ML to the Tortonian, the boundary conditions had to be adapted to the Tortonian time interval. With respect to the land–sea distribution, the present-day land–sea mask was used which is justified in view of the model resolution (see above) and the minor plate tectonic movements that occurred since the Tortonian (e.g., Ruddiman and Kutzbach, 1989; Prell and Kutzbach, 1992; Ramstein et al., 1997). However, the altitudes of the mountain chains were changed according to the Tortonian situation. They were

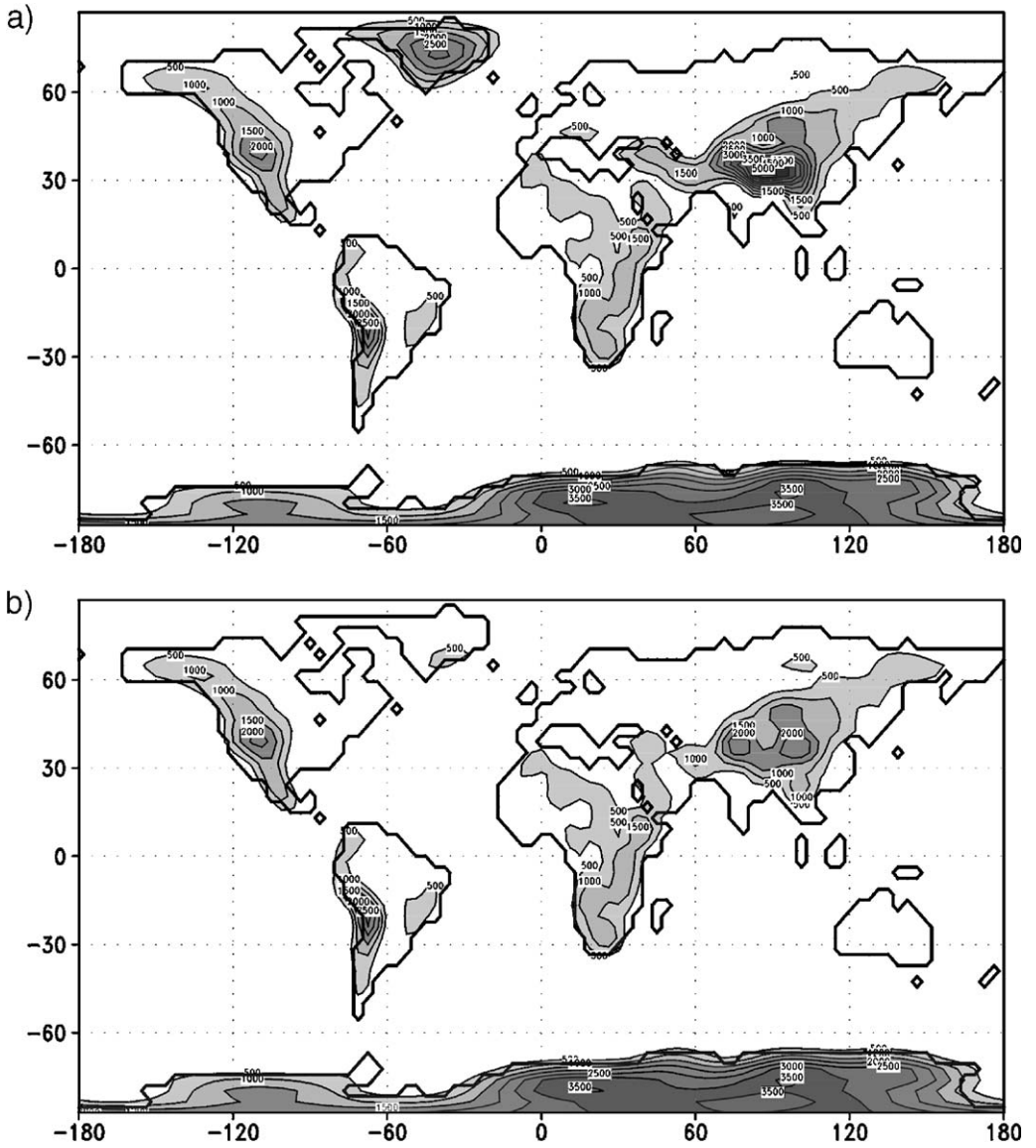

Fig. 1. The orography of ECHAM4/ML in resolution of T30 (~3.75°) of (a) the Control run and (b) the Tortonian run with changes based on geological proxy data. Represented values are Fourier transformed from spectral to grid units.

derived from geological proxy data representing the orography for the Tortonian (Kuhlemann, personal communication, a compilation of the relevant literature is available from the authors). Moreover, Greenland was considered ice-free and covered by a tundra vegetation. Based on isostatic assumptions, Greenland's Late Miocene orography–apart from its most southern regions–was calculated to reach about 10% of today's height. The orography of the Tortonian (Fig. 1) differed from the recent situation primarily by a noticeable reduction of some high mountain ranges like the Alps, Greenland and the Himalayan. The uplift of the Tibetan Plateau during the Neogene was discussed by several authors (e.g., Molnar et al., 1993; Wang et al., 1999) resulting in different mean heights of the Tibetan Plateau for the Latest Miocene. In accordance with other authors (e.g., Prell and Kutzbach, 1992), the height of the Tibetan Plateau of the Tortonian was assumed to have reached about 50% of its recent height.

We also had to adapt the ECHAM/ML to the Tortonian oceanic conditions. For this purpose, the flux correction and, thus, the oceanic heat transport had to be adjusted. This was done on the basis of palaeo-SSTs derived from δ^{18}O-data. Only few Tortonian SST data were available which, in addition, were unequally distributed on a global scale. Therefore, we devised a method to compare highly resolved recent and sparse palaeo-SSTs. The main idea is based on the meridional gradient of the SSTs which is interpreted as a measure of the heat transfer by water. In the following paragraphs, it will be outlined how palaeo-SST gradients for the Tortonian were obtained and how they were used to determine the palaeo-flux correction.

3. Determination of the palaeo-flux correction

The oxygen isotope composition of carbonates offers a good possibility for the reconstruction of palaeotemperatures (e.g., Rye and Sommer, 1980; Faure, 1986; Attendorn and Bowen, 1997; Rohling and Cooke, 1999). Being interested in palaeo-SSTs, the attention of the investigation is focused on calcareous shells of planktonic foraminifera as they represent best the conditions of the uppermost ocean layer. The δ^{18}O-values of planktonic foraminifera from Tortonian sediments were taken from publications based on ODP and DSDP sites; a total of 56 data points were available (Fig. 2). From the oxygen isotope data, palaeotemperatures were calculated using the empirical equation of Erez and Luz (1983):

$$T(\text{in}^\circ\text{C}) = 17.00 - 4.52(\delta_c - \delta_w) + 0.03(\delta_c - \delta_w)^2 \qquad (2)$$

where δ_c is the δ^{18}O composition of foraminifer carbonate (versus PDB) and δ_w is the δ^{18}O composition of sea water (SMOW). In general, accumulation of ^{18}O in the shell material decreases with increasing temperature. Zachos et al. (1994) used this equation for Palaeogene and Neogene studies showing a good

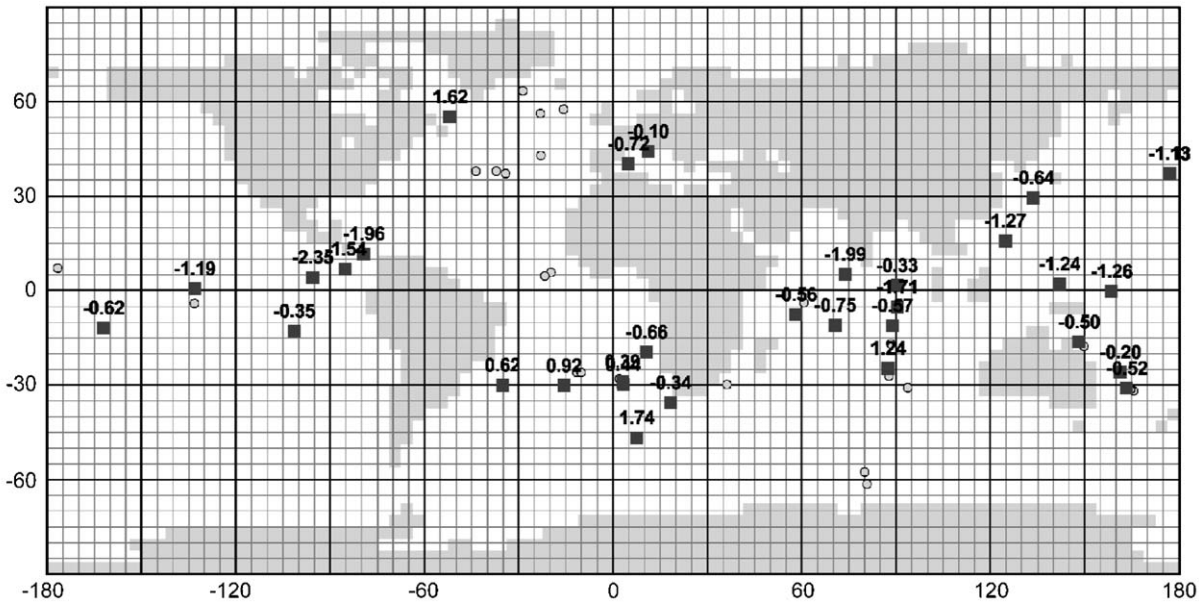

Fig. 2. The global distribution of planctonic (squares) and (benthic) (circles—partly overlapped by squares and not complete) δ^{18}O data [‰] at 8 Ma from ODP and DSDP sites.

agreement between temperature reconstructions of a Cenozoic ocean and other proxy data.

However, it is important to note that Eq. (2) may include some systematic errors. For instance, the biology of foraminifera may influence the oxygen isotope composition of the shell ('vital effect', e.g., Erez and Luz, 1983; Hemleben et al., 1989; Norris et al., 1994; Niebler, 1995; Berberich, 1996). Similarly, diagenetic effects may alter the oxygen isotope composition of the shells after the death of the organisms (e.g., Pearson et al., 2001). Moreover, the average isotopic composition of the Tortonian sea water may differ from the present and the same is true for the local salinity which varies with precipitation, evaporation and freshwater influx and directly influences the oxygen isotope composition of foraminifera shells (e.g., Craig and Gordon, 1965; Savin et al., 1985; Wolf and Thiede, 1991; Zachos et al., 1994; Nikolaev et al., 1998). According to Broecker (1989), the latitudinal variation of salinity can be taken into account with the following equation:

$$\delta_w = 0.576 - 0.041y - 0.0017y^2 + 1.35 \cdot 10^{-5} y^3 \qquad (3)$$

where y represents the absolute latitude between 0° and 70°. The validity of this formula was confirmed by Zachos et al. (1994). Hence, we also used Eq. (3) in our calculation of Tortonian SSTs to account for the latitudinal variation of salinity.

To allow for a comparison with recent SST data, the palaeotemperatures were zonally averaged with a resolution of 2°. The zonally averaged Tortonian SSTs are shown in Fig. 3. To obtain a similar recent SST data set, we used satellite data of the years 1979 to 1993 with a horizontal resolution of 2° (e.g., Woodruff et al., 1993). As for the palaeo-data, the observed satellite SSTs were zonally averaged. Additionally, we extracted from the satellite data the recent SST for all borehole locations providing Tortonian oxygen isotope data. Thus, three data sets were obtained: the zonally averaged palaeotemperatures, the zonally averaged Recent SSTs derived from satellite data, and the recent SSTs at the borehole locations also derived from satellite data. From Fig. 3, it can be seen that in mid-latitudes of the Northern Hemisphere, palaeotemperatures were generally higher than recent temperatures at the boreholes. In contrast, the subtropics and tropics tended to be slightly cooler in the Tortonian. It is possible that the slightly lower temperatures in the tropics during the Tortonian were caused by one of the above-explained sources of errors which may occur when reconstructing palaeo-SSTs from oxygen isotope data. In order to minimise such errors, the present study was focused on the meridional temperature

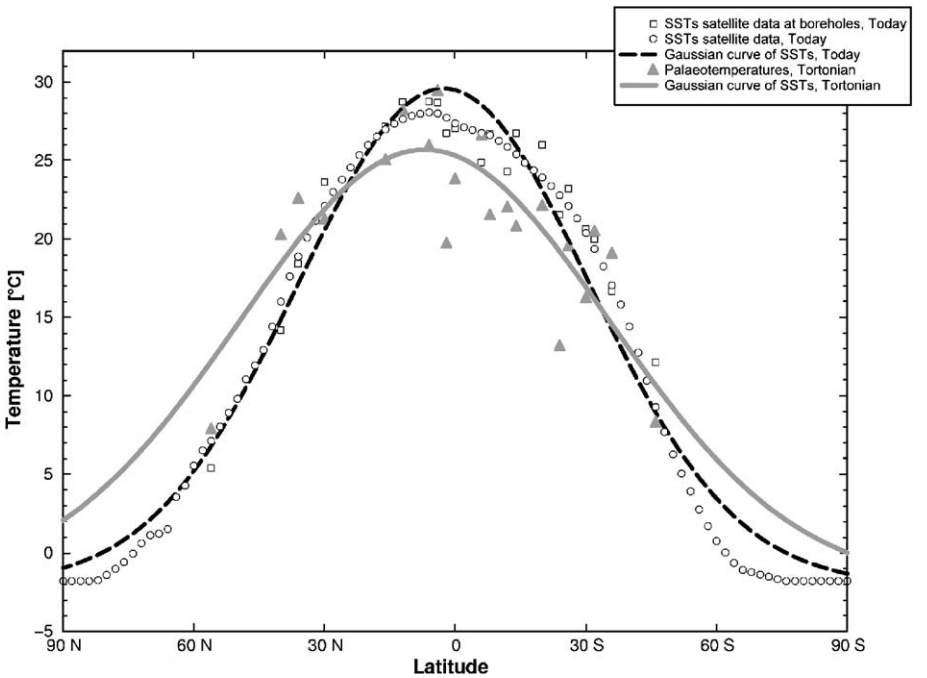

Fig. 3. The annual and zonal average SSTs from satellite data and palaeotemperature equations with corrected δ values. Circles: satellite data at borehole locations where $\delta^{18}O$ values were taken from, triangles: palaeo-SSTs received from Eqs. (3.1) and (3.2), dashed line: Gaussian curve of satellite data and solid line: Gaussian curve from palaeotemperatures.

gradient rather than on the absolute palaeotemperatures. Unfortunately, the SST information for the Tortonian is too scarce on a global scale to determine the meridional temperature gradient for all latitudes. As is evident from Figs. 2 and 3, the boreholes are mostly located between 30° northern and southern latitude and show a very uneven geographic distribution.

Hence, a method was needed to fill the geographic gaps between the available palaeo-SSTs. Our method to realise this is based on a comparison of recent and palaeo-SSTs. First, the zonally averaged temperature distribution was assumed to follow a Gaussian curve (Fig. 3). To find the best fit Gaussian curve, the method of the smallest squares was applied and, in addition, the curve was constrained by defining the minimum temperature of sea water to be −1.8 °C because of ice formation below this temperature. Using these constraints, there remain three independent parameters describing the Gaussian curve of each data set: The amplitude A, the distance from the maximum value to the reversal points σ and the latitudinal shift Δ.

The next steps in our method are illustrated in Fig. 4, where the bold-framed rectangles represent the available data sets and the shaded box represents the data set which was finally needed for the calculation of the palaeo-flux correction. The satellite data were split into annual and seasonal averages, whereas palaeo-data referred to mean annual SSTs only (the latter is due to the fact that the oxygen isotope composition of foraminifera shells reflects the mean annual temperature only). For the recent zonal average data and the recent borehole data, two Gaussian curves were calculated. Then, a transformation was determined explaining the variation of the Gaussian parameters A, σ and Δ of the recent data set based on the borehole localities as compared to the recent data set based on all latitudes. This transformation is given by a linear series expansion:

$$\begin{pmatrix} A \\ \Delta \\ \sigma \end{pmatrix}_{\text{all}} = a + b \cdot \begin{pmatrix} A \\ \Delta \\ \sigma \end{pmatrix}_{\text{loc}} + \ldots \qquad (4)$$

Therein, the index *all* describes the Gaussian parameters of the recent zonal average data set and the parameters of the recent borehole data set are designated with the index *loc*. The progression of Eq. (4) was truncated after the second term because the precision of the solution was not increased significantly even though further terms were considered. Altogether, Eq. (4) is given five times: One time for the annual average and four times for the seasonal averages of the recent data sets. Thus, the constants a and b can be determined exactly by the set of these five equations.

Applying the same transformation by using the above determined constants a and b to the palaeo-data set, the Gaussian curve of the borehole locations was transformed into the Gaussian curve of the zonal averages. The results are shown in Fig. 3. According to this reconstruction, the meridional temperature gradient in the Tortonian was shallower than today with lower SSTs in the tropics and higher SSTs in the high latitudes.

From these Gaussian curves, which reflect the recent and palaeo-SSTs (Fig. 3), the corresponding zonal gradients were calculated and used as a basis for the adjustment of the flux correction in the mixed-layer ocean model. The ratio of palaeo-gradients and recent

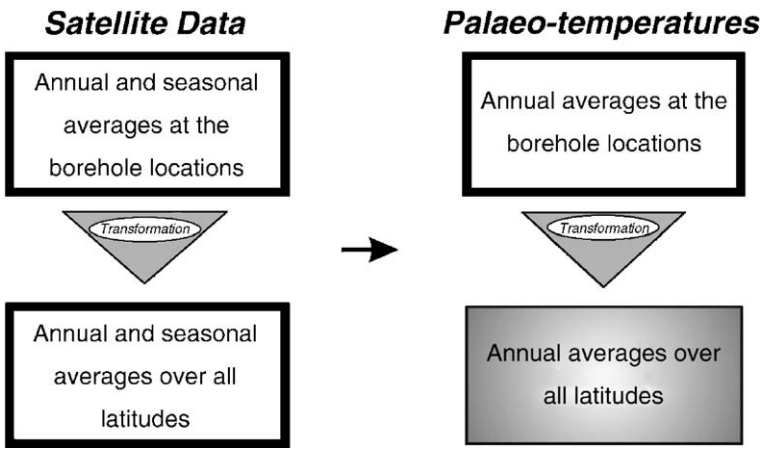

Fig. 4. Transformation scheme of the Gaussian curves. The bold-framed rectangles represent existing data sets, the shaded box represents the data set needed for the implementation in ECHAM4/ML. Transformation scheme of the Gaussian curves. The bold-framed rectangles represent existing data sets, the shaded box represents the data set needed for the implementation in ECHAM4/ML.

ones can be used as a measure of the change in heat transport to the poles and was assumed to be a zonally constant value:

$$f_0(y) = \frac{\mathrm{gradSST}(y)_{\mathrm{palaeo}}}{\mathrm{gradSST}(y)_{\mathrm{recent}}} \quad (5)$$

where the y coordinate refers to latitudes. Thereby, values of $f_0 > 1$ reflect an intensification of the oceanic heat transport in comparison to the present state whereas the oceanic heat transport is weaker, if $f_0 < 1$. Correspondingly, the palaeo-flux correction was obtained by multiplying the recent flux correction by f_0:

$$\mathrm{FC}(x,y,t)_{\mathrm{palaeo}} = f_0(y) \cdot \mathrm{FC}(x,y,t)_{\mathrm{recent}} \quad (6)$$

where the x coordinate corresponds to longitudes and t to monthly changes. It should be emphasised again that this technique was used to calculate the Tortonian flux correction and oceanic heat transport is not based on absolute SSTs but on the meridional SST gradients extrapolated by Gaussian curves from oxygen isotope data and, thus, avoids systematic errors which may occur when calculating palaeotemperatures from δ^{18}O-data. This approach, however, is based on the assumption that the near-surface palaeocean circulation was basically similar to the recent one (see Section 5 for discussion).

With regard to the oceanic heat transport, another restriction must be mentioned. The oceanic heat transport T_0 can be calculated by integrating the zonal average heat fluxes from the south to the north (e.g., Hastenrath, 1982; Carissimo et al., 1985; Hsiung, 1985; Cohen-Solal and Le Treut, 1997):

$$T_0(\phi) = \int_{\mathrm{South\ Pole}}^{\phi} \left(\int_{-\pi}^{\pi} \mathrm{div} T_0(\phi,\lambda) R \mathrm{d}\lambda \right) \cos(\phi') \mathrm{d}\phi' \quad (7)$$

wherein R designates the earth radius. The additional constraint in the determination of the flux correction was that the integral from the South Pole ($\phi = -\pi/2$) to the North Pole ($\phi = \pi/2$) must equal zero which was realised in our model.

4. Results

In the following, we compare the results from two runs with ECHAM4/ML, i.e. the Control run and the Standard Tortonian run. The Standard Tortonian run had an integration length of 30 years. After the last 20 years of simulation, the model tended to level off in an equilibrium state and, therefore, the last 10 years of integration were taken into account for a further analysis. The Control run represents the present-day situation and was taken from the experiment called EXP700-run712 (available from the DKRZ Modellbetreuungsgruppe). For the Standard Tortonian run, the Tortonian boundary conditions and flux correction were used as described above. Further, both runs used an atmospheric CO_2 concentration of 353 ppm.

We first analysed the Tortonian oceanic heat and mass transport. For this purpose, the vertical velocities and the barotropic streamfunction were calculated. Subsequently, the effect on the atmosphere was examined. For all considered parameters, we calculated the anomalies as the difference between the Tortonian and the Control run. Therefore, the seasonal and annual averages of the last 10 years of integration were calculated. The northern summer averages correspond to the months June, July and August (JJA) and the winter averages to the months December, January, and February (DJF), respectively. For the sake of brevity, only the anomalies (i.e. Tortonian minus Control run) are shown.

Corresponding to the *Central Limit Theorem*, climate variables taken over long periods tend to follow a normal distribution. Using gridded output from climate models, there are sufficient data available, both in space and time, to calculate a distribution of a variable at any grid point. In our analyses, the difference fields (Tortonian minus Control run) were computed and tested against the null hypothesis. For this purpose, a local statistical 'Student's *t*-test' (e.g., von Storch and Zwiers, 1999) was used to calculate the significance of the mean difference to zero. For the following applications, the significance level was set to $p = 0.01$.

4.1. Tortonian oceanic heat transport

The calculated Tortonian flux correction using Eqs. (5) and (6) is shown in Fig. 5. As is evident from the anomalies (Fig. 5c), the mean annual flux correction was generally weaker than today indicating a weaker oceanic heat transfer caused by the weaker meridional SST gradients (Fig. 3). For example, the Gulf Stream between 40°N and 60°N of the Tortonian study is less intense providing less energy to high latitudes of the Atlantic Ocean. The maximum reductions are in the order of 25 W/m^2. For the Kuroshio, the reductions are in the order of 31 W/m^2 providing a less intense heat transfer to the North Pacific.

The zonal average heat flux (Fig. 6) provides an overview over the changed flux correction where positive/negative values correspond to divergence/convergence zones of the implied oceanic heat transport.

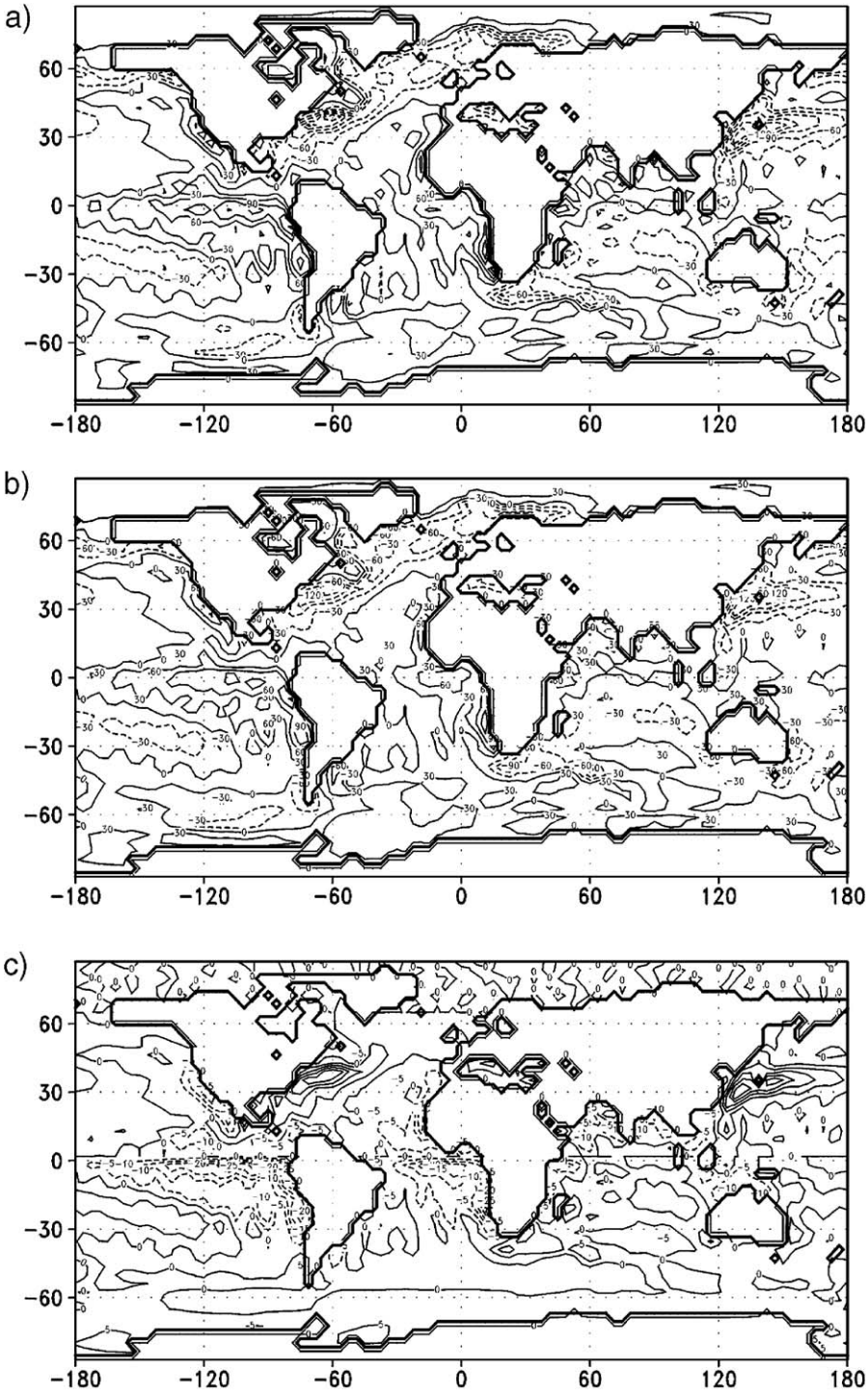

Fig. 5. The mean annual flux correction [W/m^2] for (a) the Control run, (b) the Tortonian run and (c) the difference between the Tortonian and the Control run.

The Tortonian heat flux is reduced by 7 W/m^2 in the tropics corresponding to a decreased heat divergence near the equator. In contrast, convergence is decreased by 4 W/m^2 in the mid-latitudes of the Northern Hemisphere. This corresponds to a weakened poleward oceanic heat transport.

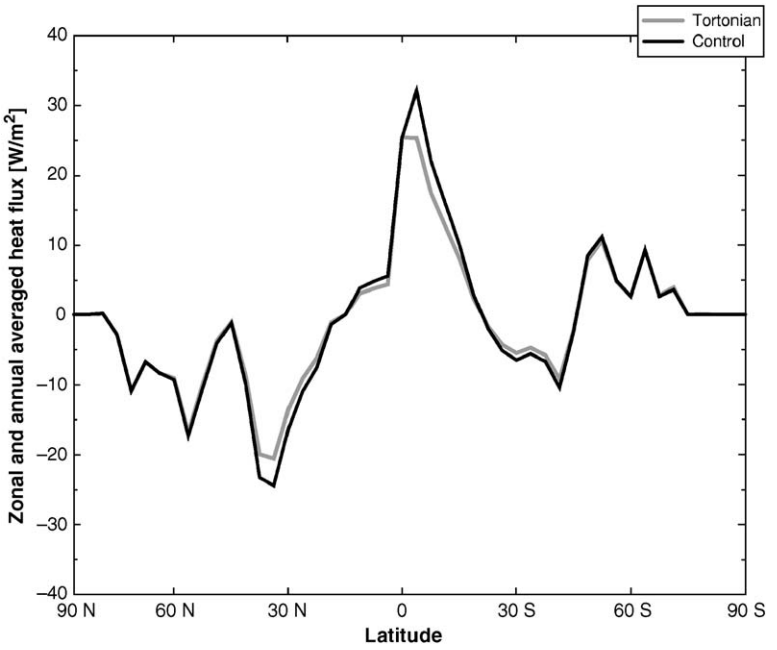

Fig. 6. The zonal and annual average divergence of the oceanic heat transport. Black solid: Recent curve, grey solid: Tortonian curve.

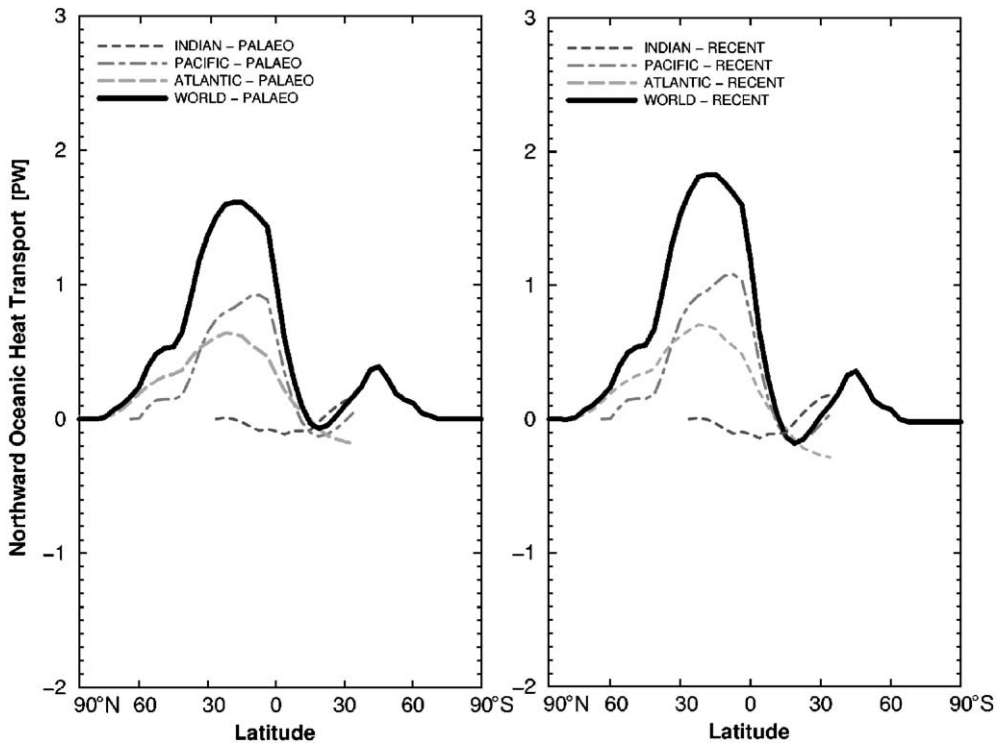

Fig. 7. The northward oceanic heat transport [PW] of the world ocean and the main basins splitted into nowadays (right) and the Tortonian (left) transport.

In Fig. 7, the calculated oceanic heat transport T_0 is shown (Eq. (7), e.g., Hastenrath, 1982; Carissimo et al., 1985; Hsiung, 1985; Cohen-Solal and Le Treut, 1997). The present-day's oceanic heat transport has a maximum around 20°N (Fig. 7, right side). The position and absolute value of the maximum complies with studies of several

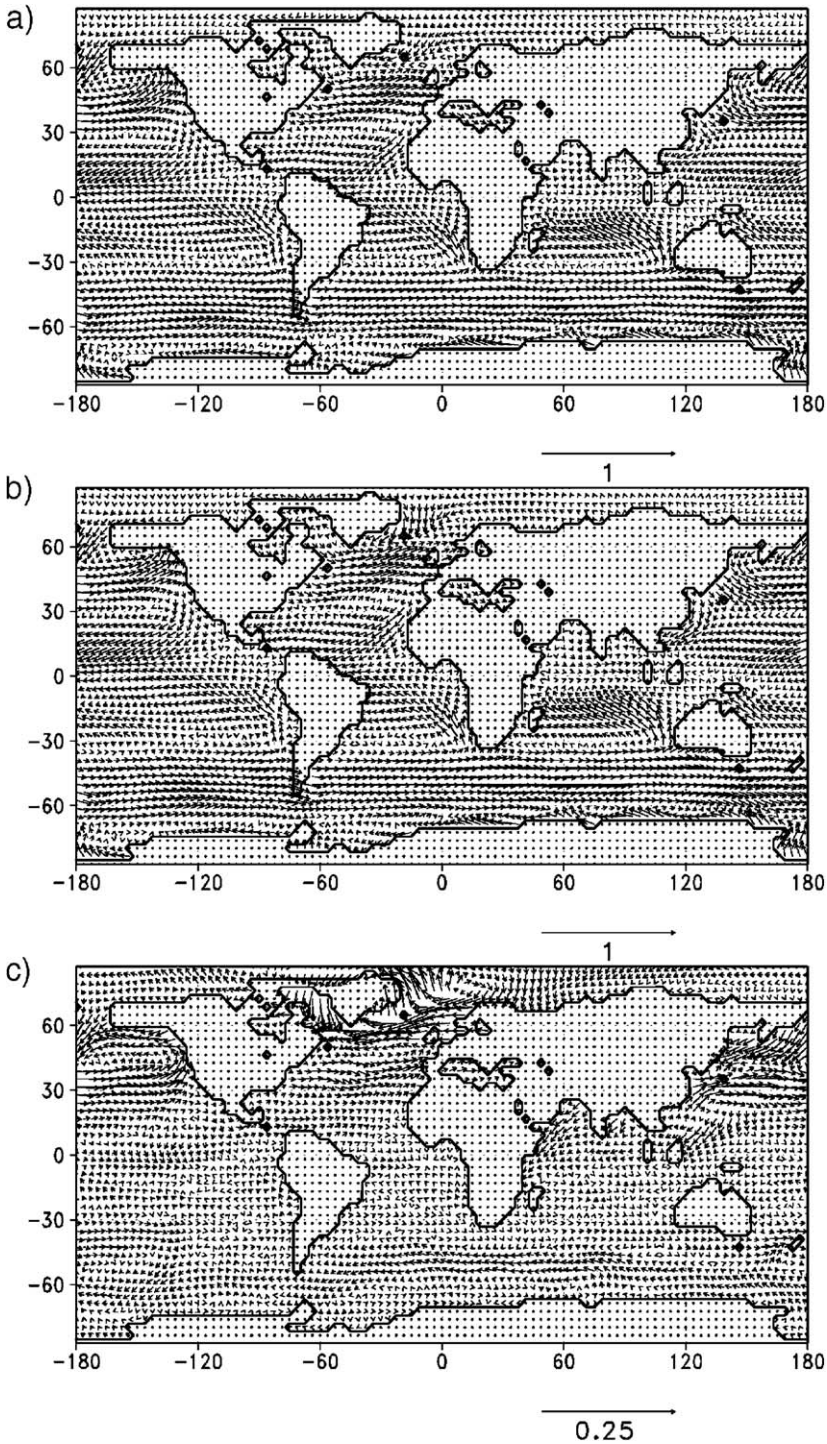

Fig. 8. The mean annual wind stress field corresponding to (a) the Tortonian run, (b) the Control run and (c) the difference between the Tortonian and the Control run. The magnitude of the reference arrow is 1 m/s for (a) and (b), and 0.25 m/s for (c).

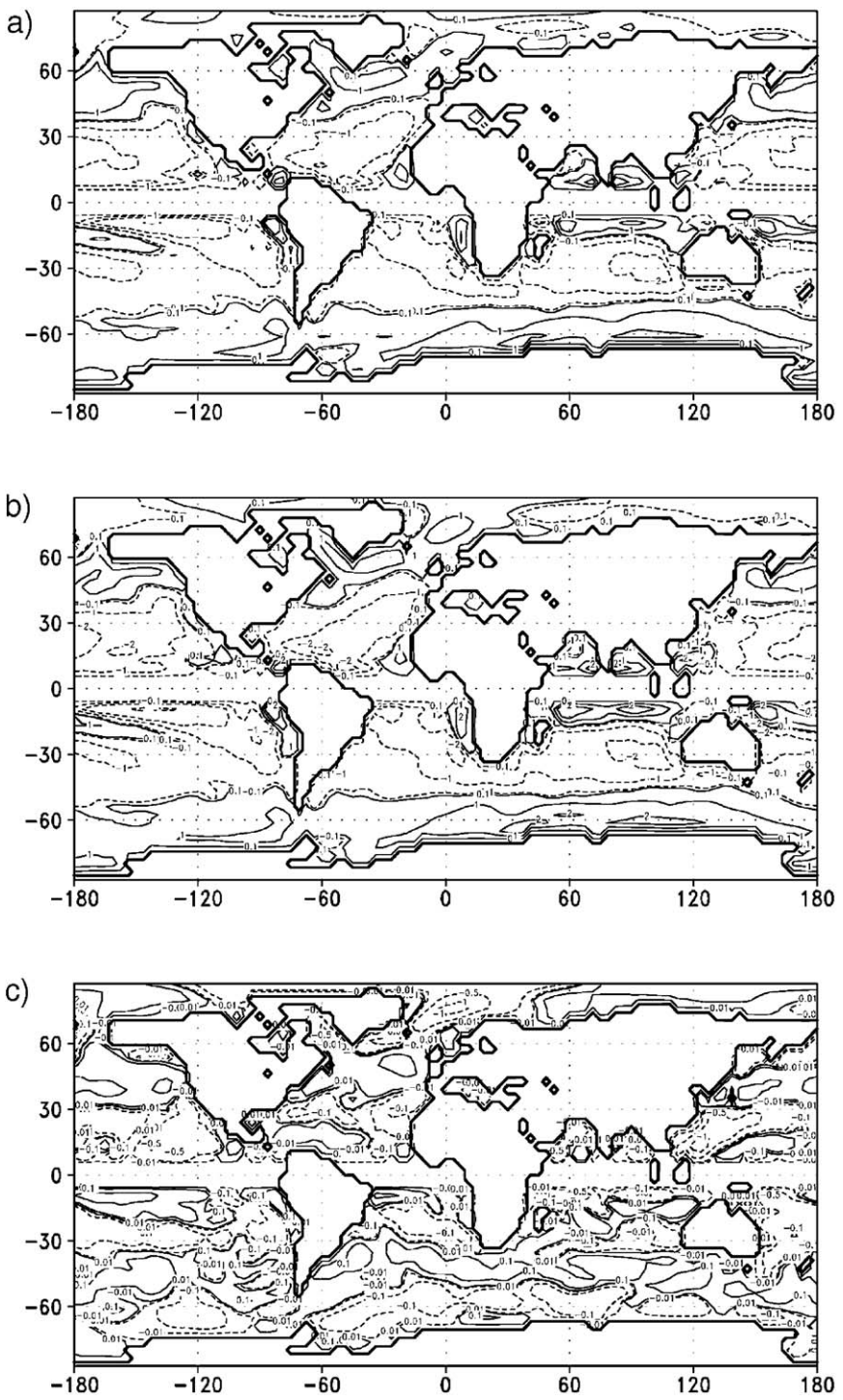

Fig. 9. The vertical velocities at the base of the Ekman layer [$\times 10^6$ m/s]. Positive/negative values correspond to upwelling/downwelling areas. (a) The Tortonian run, (b) the Control run, and (c) the difference between Tortonian and Control run. Contour intervals are −5, −2, −1, −0.1, 0.1, 1, 2, 5×10^6 m/s for (a) and (b), and −5, −1, −0.5, −0.1, −0.01, 0.01, 0.1, 0.5, 1 and 5×10^6 m/s for (c). The vertical velocities at the base of the Ekman layer [$\times 10^6$ m/s]. Positive/negative values correspond to upwelling/downwelling areas. (a) The Tortonian run, (b) the Control run, and (c) the difference between Tortonian and Control run. Contour intervals are −5, −2, −1, −0.1, 0.1, 1, 2, 5×10^6 m/s for (a) and (b), and−5, −1, −0.5, −0.1, −0.01, 0.01, 0.1, 0.5, 1 and 5×10^6 m/s for (c).

other authors (e.g., Carissimo et al., 1985; Gleckler et al., 1995). For instance, other authors estimated the maximum recent meridional heat transport of the world ocean to be between 1.5 and 2.5 PW (e.g., Ganachaud and Wunsch, 2000). A value in the order of 1 PW at 24°N was suggested by Roemmich and Wunsch (1985).

For the Tortonian (Fig. 7, left side), the northward oceanic heat transport is weakened in comparison to the control run which is due to the changed flux correction. The maximum values for the Tortonian world ocean on the Northern Hemisphere are reduced by approximately 0.2 PW resulting in lower poleward heat transport. Focusing on the North Atlantic, the meridional oceanic heat transport is reduced by about 0.1 PW. With regard to the Pacific Ocean, differences between recent and Tortonian oceanic heat transport are of the same order of magnitude.

4.2. Tortonian oceanic mass transport

To investigate the horizontal and vertical mass transports in the ocean, the surface wind stress field has to be considered (Fig. 8). The mean annual wind stress of the Control run is widely consistent with wind stress data derived from surface wind analysis (Hellermann and Rosenstein, 1983; Trenberth et al., 1990). For example, formation of subtropical gyres related to trade winds and strong westerly components at mid-latitudes of both hemispheres are well represented. However, even small differences in wind stress may have an impact on the ocean circulation (Townsend et al., 2000).

The comparison between Tortonian and Control run shows only small differences in the wind stress patterns. For instance, a decrease in wind stress at high mid-latitudes of both hemispheres is observed (Fig. 8c). With regard to the low mid-latitudes of the North Pacific and the North Atlantic, an increasing wind stress occurs and should induce a strengthening of ocean currents. Calculations of several authors (e.g., Leetmaa and Bunker, 1978; Trenberth et al., 1990; Danabasoglu, 1998; Townsend et al., 2000) show the linkage between the climatological wind stress field at the ocean surface and the wind driven horizontal and vertical oceanic circulation. Using the wind stress curl, the vertical velocity fields for the Tortonian and Control run were calculated (Fig. 9). For both runs, strong upwelling zones are identified at the eastern margins of the southern ocean basins. Moreover, water which is upwelled in the tropics is transported to the subtropics where it sinks. The vertical velocities of the recent Control run show larger absolute values. This indicates a weaker wind-induced ocean circulation during the Tortonian. The calculated vertical velocities near the ice edge around Antarctica are, however, not realistic as the wind stress there rather represents movements of the ice sheets than movements of the ocean water.

The differences between the Tortonian and Control run with respect to the vertical velocity field are relatively small for the tropical upwelling zones at the eastern margins of the South Atlantic and South Pacific Ocean (Fig. 9). For the Tortonian, these regions show an increase

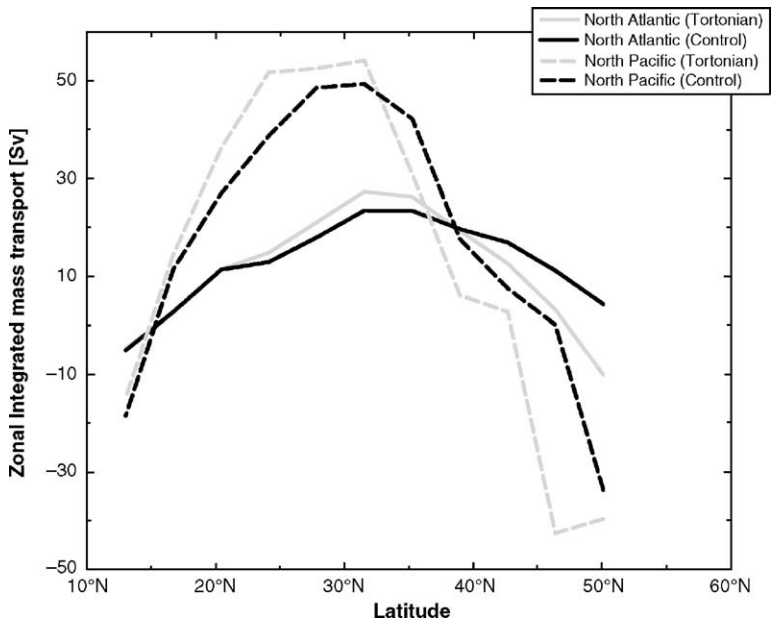

Fig. 10. The annual average Sverdrup transport streamfunction in [Sv] over the global oceans.

of upwelling in their central areas and a significant decrease of upwelling in the surrounding areas to the west. This indicates a shortening of the currents at the eastern continental margins but their intensity is locally increased. In the subtropics, negative vertical velocities are intensified corresponding to an increased downwelling in particular in the subtropical North Pacific and North Atlantic. This is caused by the increased surface wind stress which, due to the conservation of mass, leads to an intensified downwelling.

As a quantitative measure of the oceanic response to the atmospheric forcing, the Sverdrup transport is considered. Since a mixed-layer ocean is used, the mass transport is calculated with the surface wind stress curl. Thus, the equatorial return flows of the intermediate and the deep water are not considered. Here, the investigation was focused on the ocean currents of the Northern Hemisphere: the Gulf Stream and Kuroshio. For the Control run mean annual values of 23.5 Sv and 49.3 Sv, respectively, were obtained. Roughly the same values were calculated by Harrison (1989) and Townsend et al. (2000) for the Recent. The Tortonian run differs with respect to the northward transport of ocean water (Fig. 10). The northward flow of the currents at the western margins is strengthened at lower latitudes because of the increased surface wind stress of the Tortonian run. At higher latitudes, however, the oceanic mass flux is weakened. The general pattern shows an equatorial shift of maximum transport along the western margins with a reduced Sverdrup transport further northwards. This is consistent with a shortening of the Gulf Stream and a reduction of oceanic heat transport of the Northern Hemisphere (Section 4.1).

4.3. Global temperature and Sea ice patterns

Surprisingly, the temporal evolution of the globally averaged surface temperature (Fig. 11) does not show

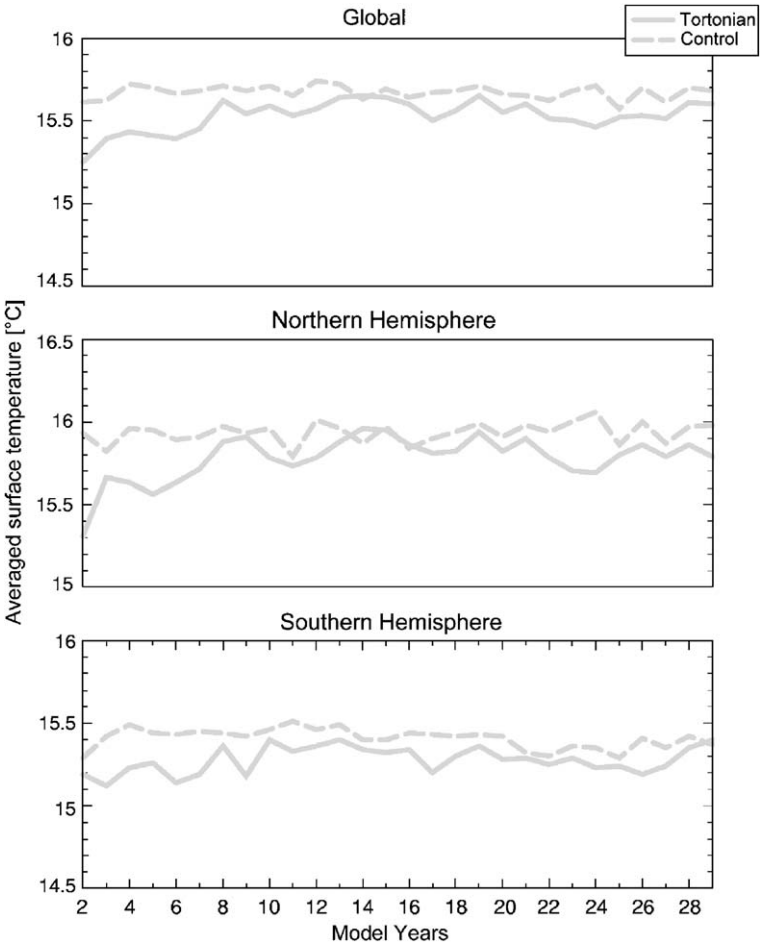

Fig. 11. The annual and global average surface temperature [°C] using weighted areas of the Tortonian (grey solid) and the Control run (grey dashed).

significant differences between Control and Tortonian run. The distribution of sea ice is another important climate factor influencing both atmospheric and oceanic circulation. The differences between Tortonian and Control run with respect to sea ice are summarised in Fig. 12. For both hemispheres, there are hardly any differences in sea ice fraction, whereas the sea ice depth is decreased in the Tortonian run resulting in a noticeably reduced sea ice volume of the North Polar Sea. Obviously, the elimination of the Greenland ice sheet contributed to this reduction of sea ice.

4.4. Atmospheric patterns

In the following, the large scale atmospheric patterns are described. In spite of the almost unchanged globally averaged surface temperatures (Fig. 11), there are significant differences in the near surface temperature patterns in particular over continental areas (Fig. 13). In general, the Tortonian mean annual, winter and summer temperature in the Northern Hemisphere show an increase at high latitudes and a decrease at mid-latitudes (Fig. 13c). In the Southern Hemisphere, differences between the Tortonian and Control run are less significant. There is a slight temperature increase over parts of the subtropical oceans and near the margin of sea ice. In contrast, over Antarctica a cooling occurs which is more intense during the southern winter (Fig. 13a).

In accordance with the decreasing sea ice volume of the Northern Hemisphere (Fig. 12), there is an enormous temperature increase over and surrounding Greenland caused by the removal of the inland ice. For the Tortonian run, however, mean annual

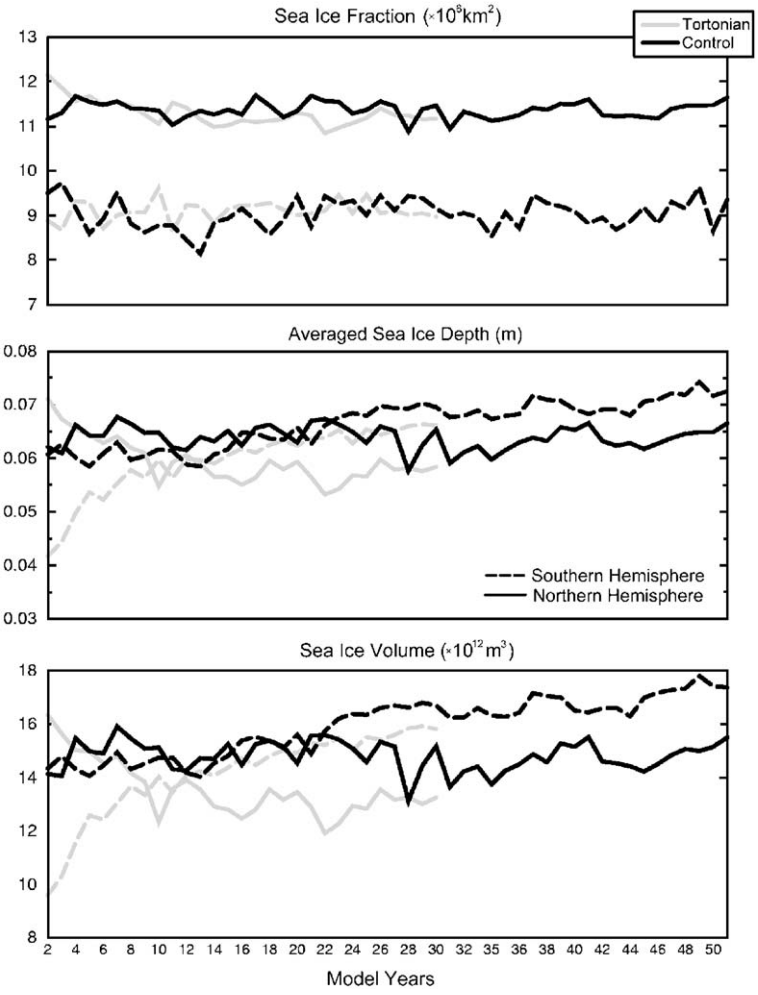

Fig. 12. The annual average global sea ice fraction [$\times 10^6$km^2], sea ice depth [m] and sea ice volume [$\times 10^{12}$m^3] of both hemispheres. Dashed: Southern Hemisphere, solid, Northern Hemisphere, black: Control run, grey: Tortonian run.

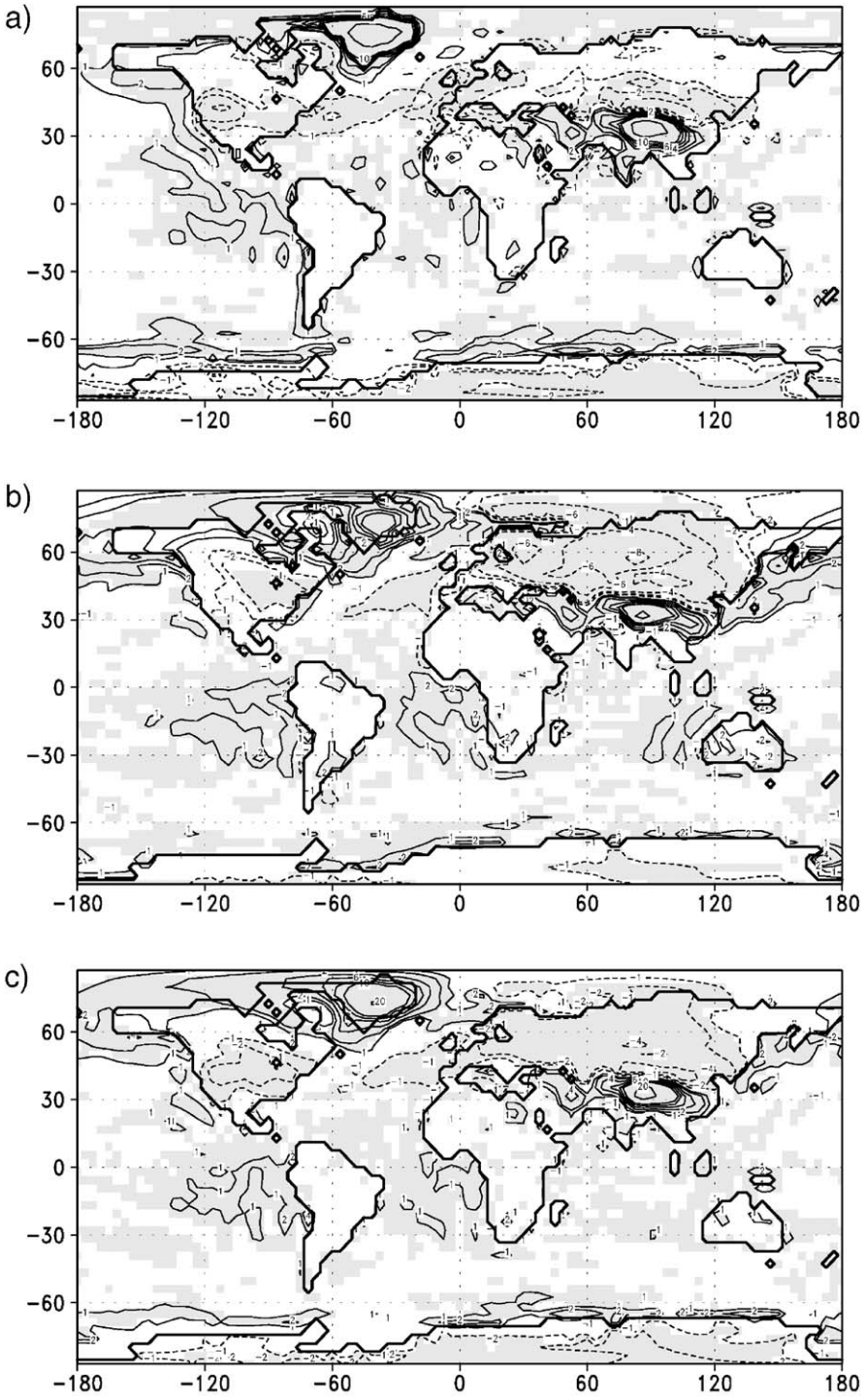

Fig. 13. The averaged surface temperature anomalies [°C] between the Tortonian and the Control run for (a) JJA, (b) DJF, and (c) the annual average. Shaded areas represent 'highly significant' anomalies with a local 'Student's *t*-test' ($p < 1\%$).

temperature values in Greenland are still below zero. Over the ocean around Greenland, the increase in temperature can be attributed to the positive feedback mechanism of the ice-albedo effect. In addition, the temperature anomalies vary with the seasons. Regarding the near-surface temperatures over the polar ocean,

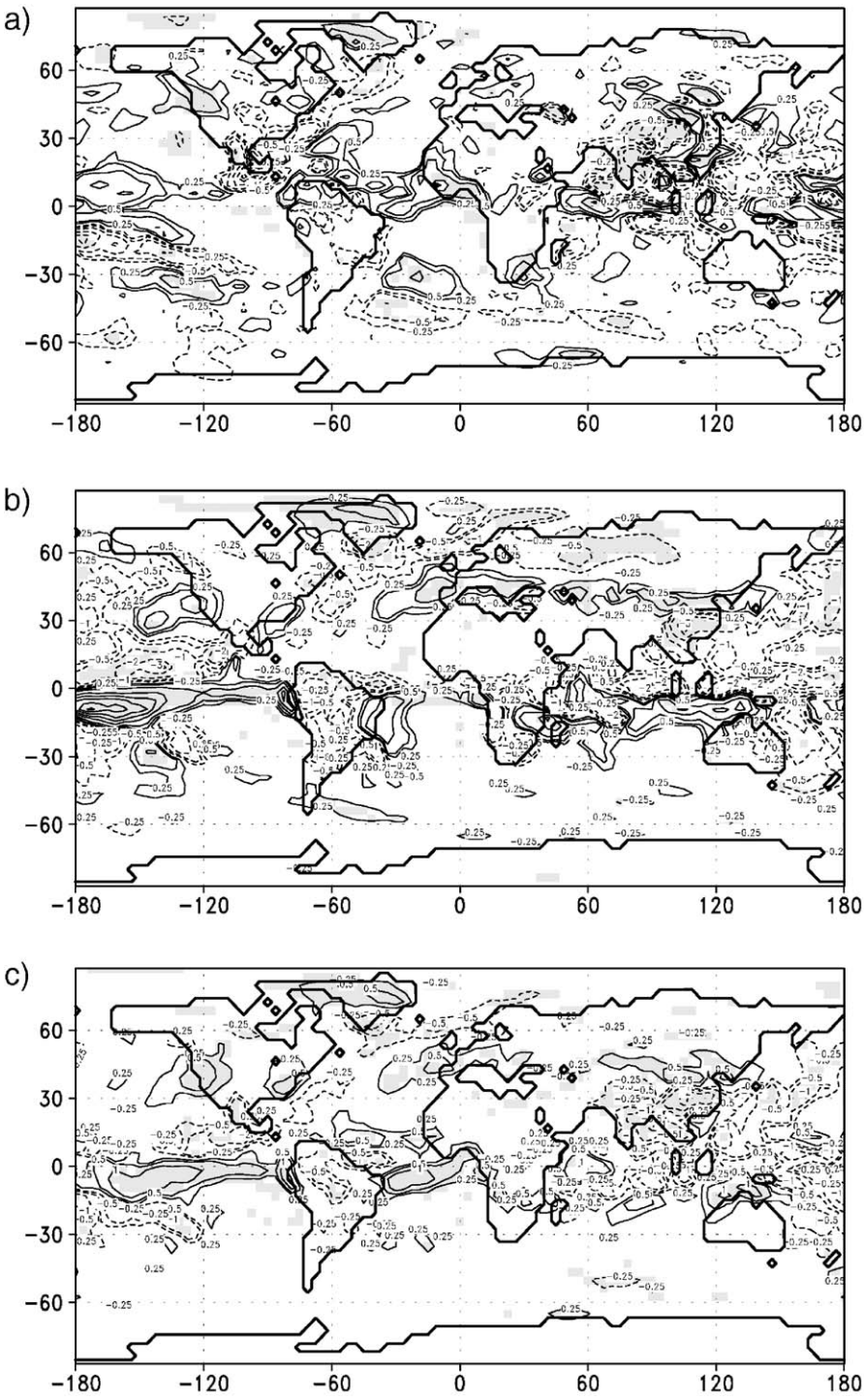

Fig. 14. The averaged anomalies of the precipitation rates [mm/day] between the Tortonian and the Control run for (a) JJA, (b) DJF, and (c) the annual average. Shaded areas represent 'highly significant' anomalies with a local 'Student's *t*-test' ($p<1\%$). The averaged anomalies of the precipitation rates [mm/day] between the Tortonian and the Control run for (a) JJA, (b) DJF, and (c) the annual average. Shaded areas represent 'highly significant' anomalies with a local 'Student's *t*-test' ($p<1\%$).

the warming during winter months is stronger (Fig. 13b) than during summer (Fig. 13a), similarly, the Antarctic cooling appears more intense during summer than during winter. Thus, the Tortonian seasonality is reduced in the high latitudes. In combination with the temperature rise over Greenland, the precipitation rate

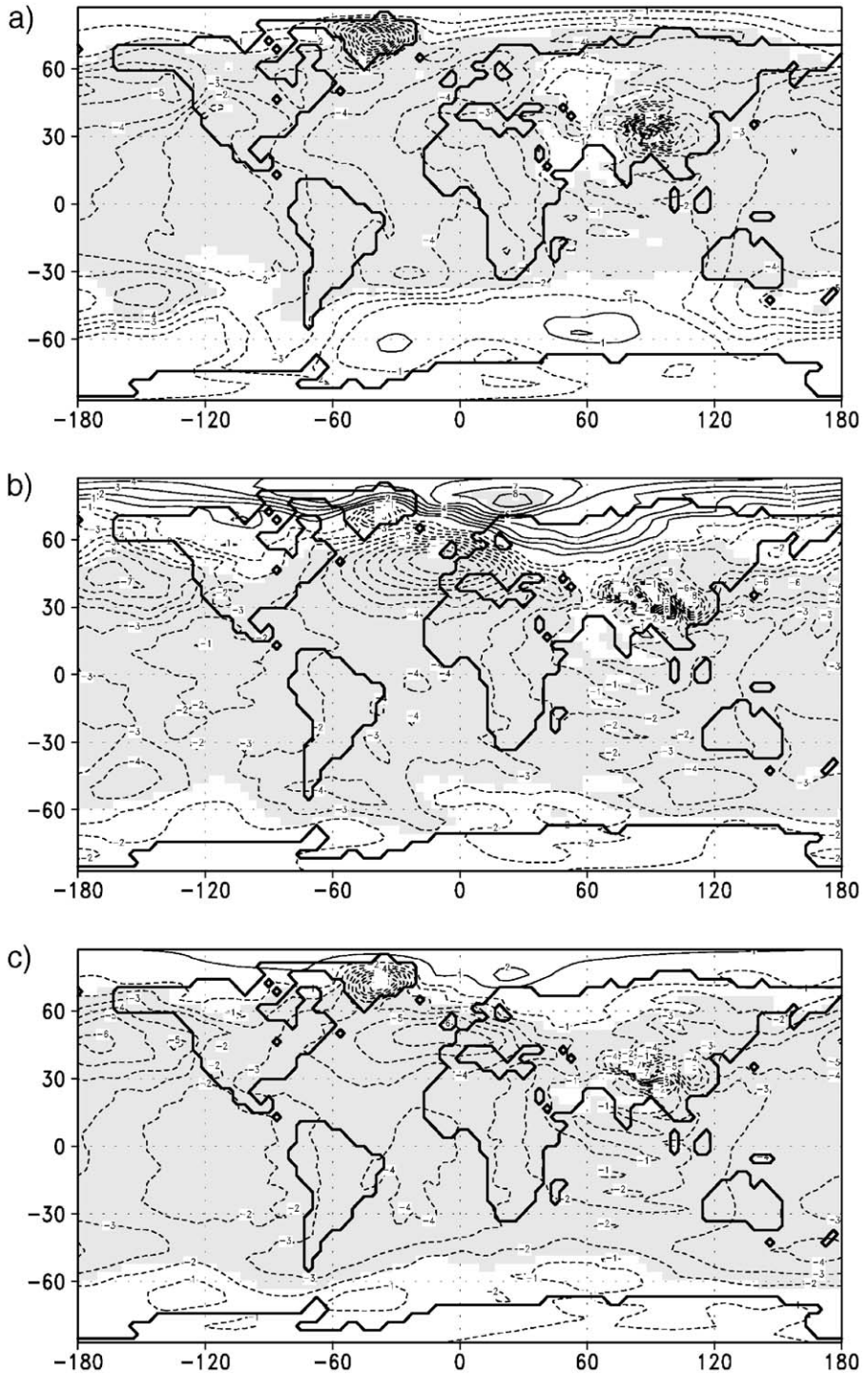

Fig. 15. The averaged anomalies of the surface pressure [hPa] between the Tortonian and the Control run for (a) JJA, (b) DJF, and (c) the annual average. Contour interval is 1 hPa. Shaded areas represent 'highly significant' anomalies with a local 'Student's *t*-test' ($p < 1\%$).

is significantly increased over land (Fig. 14). A summer precipitation increase of up to 108 mm corresponds to an amplification of 300%.

For the Tortonian run, mid-latitudes are characterised by significantly lower temperatures (Fig. 13). This decrease can partly be attributed to the change in the

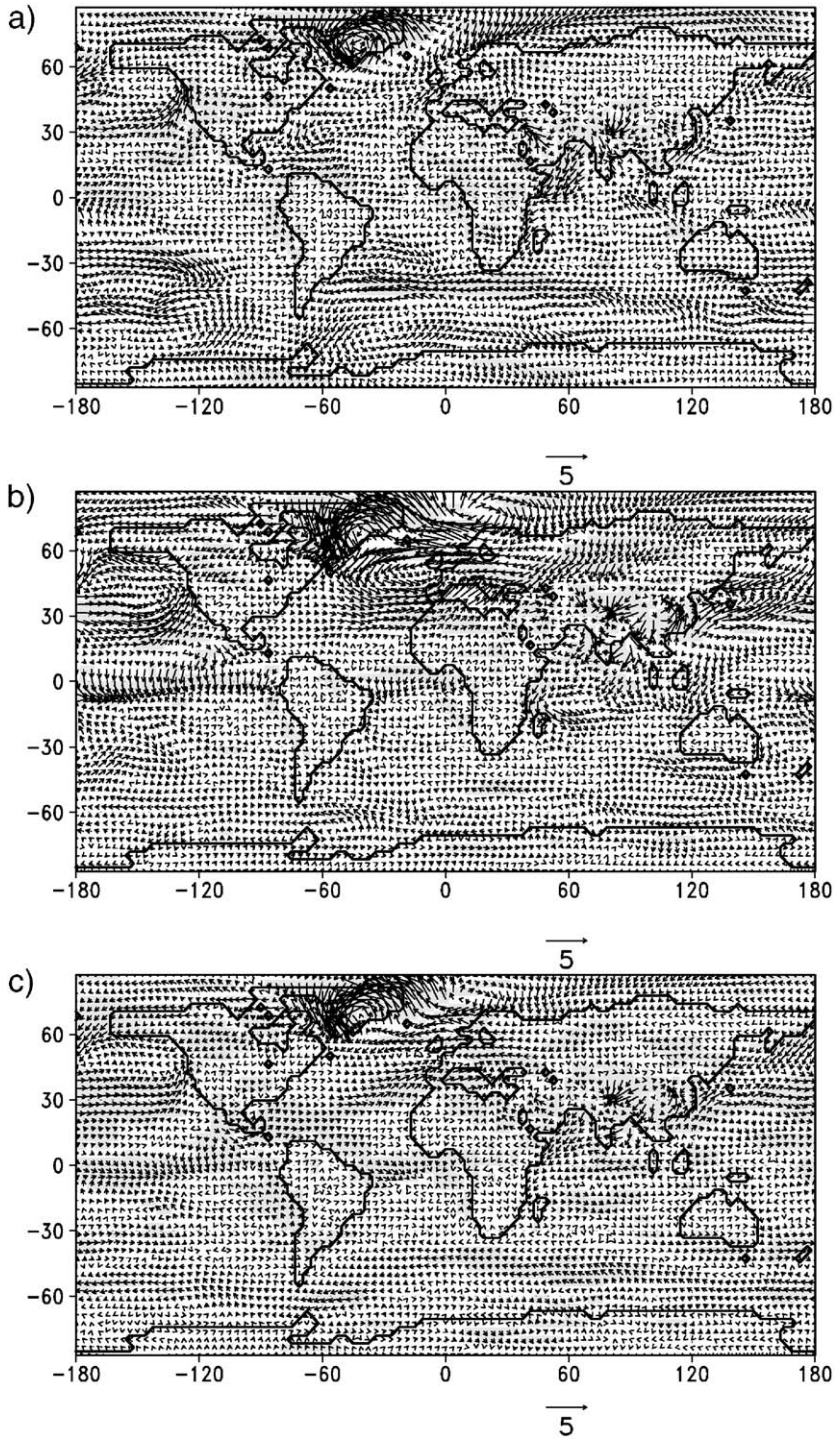

Fig. 16. The averaged anomalies of the wind vectors [m/s] between the Tortonian and the Control run for (a) JJA, (b) DJF, and (c) the annual average. The reference arrow is representing 5 m/s. Shaded areas represent 'highly significant' anomalies with a local 'Student's *t*-test' ($p < 1\%$).

oceanic heat transport. The northward oceanic heat transport is reduced resulting also in a reduction of the Gulf Stream. Hence, less heat is transferred to Central and Northern Europe. Consequently, continental areas in Asia are also provided with colder air masses. Whereas continental areas become slightly cooler in Asia, the average temperatures over the Himalayas are strongly enhanced (about 20 °C in maximum) which is due to the reduced Tortonian orography. In contrast to this, the annual precipitation pattern in Southeast Asia shows at the same time a reduced rainfall of about 400 mm/year or more. This decrease is noticeable during summer especially with a reduction of more than 200 mm/month as a maximum. This feature indicates a weaker Tortonian monsoon system in our model. As the Gulf Stream is more effective during winter, a strong cooling during DJF (December, January, February) occurs over the Eurasian continental regions. Over the North Atlantic, the temperature gradient from mid-latitudes to high latitudes is reduced. This complies with the prescribed oceanic heat transport. However in the subtropics, the temperature gradient is slightly increased leading to an intensified oceanic mass transport (Fig. 10).

There is also an amplification of the Iceland Low over the North Atlantic which is seen from the differences in the sea surface pressure (Fig. 15). This indicates an increased atmospheric cyclonic character during winter. Consequently, the surface wind is amplified from the North Atlantic region to Southern Europe (Fig. 16) and, as a result, precipitation in Southern Europe is increased by 144 mm/year to 1116 mm/year.

With regard to the Pacific Ocean, the atmospheric circulation of the Tortonian run differs from the Control run. A changed atmospheric flow is indicated by the mean annual temperature anomalies (Fig. 13) over the central and eastern Pacific Ocean. These differences correlate with the El Niño-year pattern well known from recent observations and climate modelling (e.g., Latif and Neelin, 1994; Bigg, 1999). In general, recent climate measurements show positive temperature anomalies of about 2–4 °C of the upper 50 m in the ocean during DJF. In contrast to Tortonian results, these temperature variations occur on a time period of 2–8 years (Timmermann et al., 1999). For the Tortonian run, there is a significant warming of more than 2 °C at the eastern margin of the Pacific Ocean. The warming occurs in correspondence with a decreased upwelling in this coastal area. Moreover, the atmospheric circulation is also reorganised. As climate models and measurements show, an El-Niño-like pattern is combined with a weakening of the equatorial Walker circulation (e.g., Bigg, 1999). Hence, equatorial trade winds are weakened which is also evident from numerical results of the Tortonian run (Fig. 16). Consequently, a convergence zone over the central Pacific Ocean is formed resulting in a highly significant increase in precipitation (Fig. 14). Furthermore, there are drier regions over the eastern and western Pacific. A comparison of recent and palaeo model output shows that the atmospheric circulation of the Tortonian run over the Pacific Ocean equals a permanent El-Niño state. As it is analysed from present-day's climate model results (e.g., Roeckner et al., 1993), there are, in addition to tropical atmospheric responses, also extra-tropical climate changes somehow related to the El-Niño phenomenon. Carrillo et al. (2000) find that the North Atlantic storm track regimes are affected by El-Niño events. Thus, a more cyclonic character in the Standard Tortonian run (cf. above) can be related to the El-Niño-like pattern in the Pacific region, which would be consistent to the results of Carrillo et al. (2000).

5. Discussion

Our investigation of the Late Miocene climate is the first to use a coupled AGCM/ML model with a realistic and proxy-based adjustment of the flux correction; previous modelling studies for the Miocene either used modern-day SSTs or prescribed more or less arbitrarily an oceanic heat transport (e.g. Barron and Peterson, 1991; Dutton and Barron, 1997; Ramstein et al., 1997). To adjust the palaeo-flux correction we used a new method which is based on the assumptions (1) that the near-surface palaeocean circulation is basically similar to the recent one and (2) that the meridional, zonally averaged SST gradient reflects the ocean heat transport and can be used to derive the palaeo-flux correction. Thus, the calculation of the palaeo-flux correction is not based on the absolute palaeo-SSTs but on the SST-gradients. To determine the palaeo-SST gradient we used $\delta^{18}O$ values from Tortonian planktonic foraminifera. Although the calculation of palaeo-SSTs from $\delta^{18}O$ values according to Eq. (2) can be influenced by a number of effects (e.g. vital effects, diagenesis, ice volume, cf. Section 3), this should not significantly alter the estimation of the palaeo-SST gradient.

To test the robustness of our method, a control calculation was done assuming small variations of the parameters δ_c and δ_w in Eq. (2). The result of this test is shown in Fig. 17. For the calculations we considered the effect of a different oxygen isotope composition of the ocean water on the SST gradient. To represent the effect of a uni-polar ice-cover, a correction factor of −0.4‰

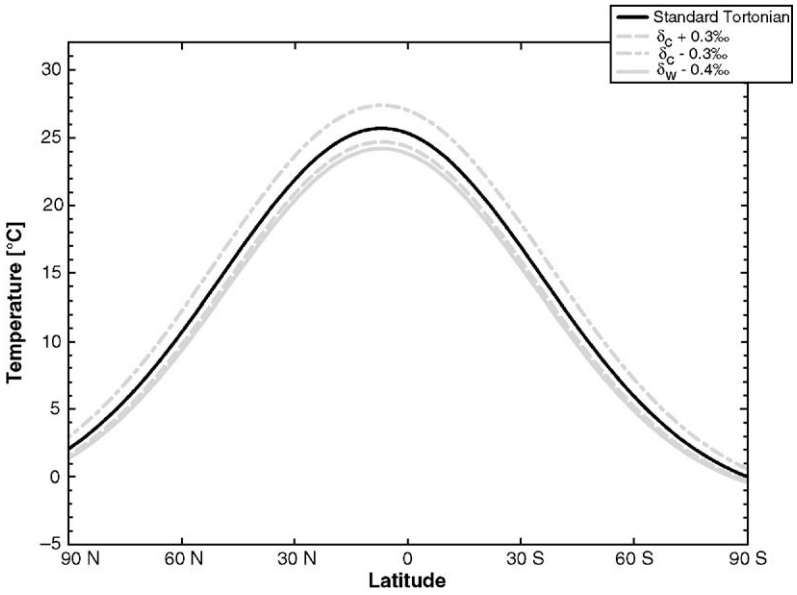

Fig. 17. The different Gaussian curves representing the meridional palaeotemperatures calculated from Eqs. (2) and (3) with differences in δ_c and δ_w values relative to the standard Tortonian temperature curve. Black solid: standard curve of the Tortonian, grey solid: an additional correction of −0.4‰ for δ_w, dashed: an additional correction of −0.3‰ for δ_c, dotted-dashed: an additional correction of +0.3‰ for δ_c.

for δ_w was used as proposed by Zachos et al. (1994). Variations in δ_c values of ±0.3‰ were also taken into account to reflect possible errors due to vital or diagenesis effects. As is evident from Fig. 17, these changes in the calculation of the palaeo-SST from δ^{18}O-values do not significantly change the shape and thus the meridional gradient of the zonally averaged SST curve. In Fig. 18, the influence of these small deviations in

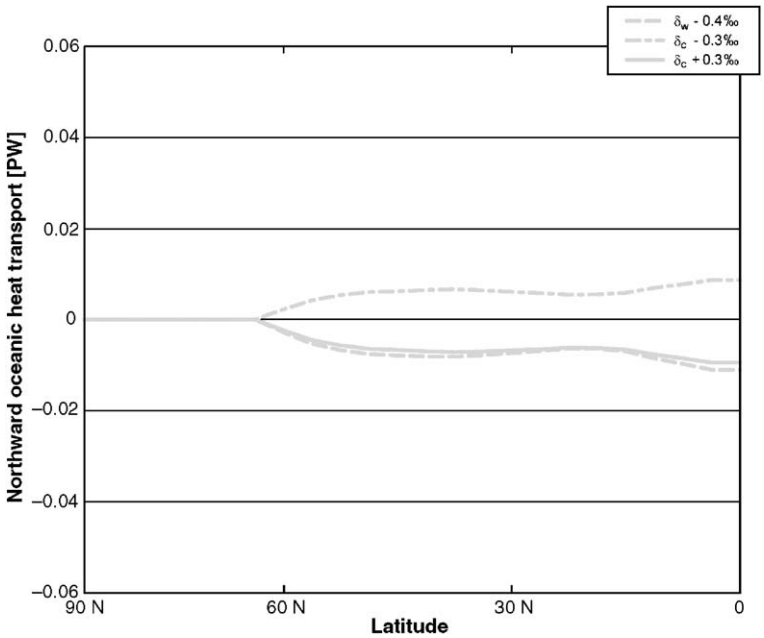

Fig. 18. The changes in the northward oceanic heat transport of the Atlantic Ocean in comparison to the standard Tortonian data base. Differences belong to deviations in δ^{18}O values. Long-dashed: deviations in δ_w of −0.4‰, dot-dashed: deviations in δ_c of −0.3‰ and solid: deviations in δ_c of +0.3‰.

δ^{18}O-values on the oceanic heat flux is illustrated for the Atlantic Ocean and adds up to less than ±0.01 PW corresponding to less than 10% of the initially calculated value. Thus, the method to derive the palaeo-flux correction is relatively robust and simple. It can be applied to different periods without much effort, provided that the two basic assumptions (see above) are valid.

With respect to the results, our analysis is largely consistent with previous modelling studies. As a consequence of the prescribed oxygen isotope data, our model shows a generally weaker northward oceanic heat and mass transport for the Tortonian (Sections 4.1 and 4.2). This is in agreement with results of e.g. Mikolajewicz et al. (1993) and Mikolajewicz and Crowley (1997) who investigated the effect of an open Panama isthmus using complex ocean circulation models (OGCMs). Obviously, significant variations in the oceanic circulation of the Neogene were caused by changes in the geometry of the ocean basins and by the closures of seaways between the Atlantic and Pacific Ocean and between the Pacific and Indian Ocean inducing the development of more intense ocean currents over the last 20 Ma (Woodruff and Savin, 1989; Maier-Reimer et al., 1990; Barron and Peterson, 1991; Flower and Kennett, 1994; Collins et al., 1996; Wright and Miller, 1996; Tsuchi, 1997; Haug and Tiedemann, 1998; Bice et al., 2000). For the Tortonian run, we did not adapt the palaeogeography, but we used Late Miocene δ^{18}O-data to adapt the flux correction of the Tortonian run. The marine isotope data represent the palaeocean circulation according to the Late Miocene ocean basin configuration (e.g. open Central American Isthmus). Hence, the adapted palaeo-flux correction also represents the effects of the palaeogeography on the Miocene ocean circulation in the Tortonian run. However, the differences in the palaeogeography as compared to the modern one can explain inconsistencies in the atmospheric patterns of the Tortonian run (see below).

Regarding the radiation budget, our Tortonian model produces no significant changes in the global mean temperature. Obviously, the climatic effects of lowered mountain ranges, such as the Himalayan, of reduced oceanic heat transport and of the lack of a Greenland ice sheet compensate each other on a global scale and do not increase the global mean temperature significantly. The meridional distribution of temperature fields, however, is changed in our Tortonian model and particularly the higher latitudes become warmer. In contrast to our results, Dutton and Barron (1997), using the model GENESIS, observed a warming of 1.9 °C for their Miocene run with modern vegetation as compared to their present-day Control run. On the other hand, they found a particular warming in the high latitudes and thus a flattening of the meridional temperature gradient as it is also obvious in our Tortonian run. The differences between the Miocene run of the GENESIS model and of our Tortonian run with ECHAM4/ML may be due to slightly different boundary conditions such as different elevations of the mountain ranges; however, they may also be caused by variations in the model physics, in particular by our method to consider the Miocene ocean properties more realistically.

As a consequence of the significant warming of the higher latitudes, our Tortonian model predicts a slightly smaller extent of the sea ice and a significant reduction of its depth. Despite a general agreement in the overall trend proxy data (e.g., Wolf and Thiede, 1991), this indicates much less sea ice in the Northern Hemisphere than modelled in our Tortonian run. Unfortunately, no precise information about the onset and development of the arctic sea ice is available because of the lack of data from the central Arctic Ocean (Thiede et al., 1998). According to Wolf and Thiede (1991), the Arctic Ocean was ice covered before 8 Ma; between 9 and 7 Ma cold ocean currents started to evolve around Greenland.

Although the Tortonian and Control run produce more or less the same global average temperature, they differ significantly in their atmospheric patterns (Section 4.4). The Tortonian model temperature of the northern high latitudes is significantly warmer than today but differences are less evident in the Southern Hemisphere. This pattern is only partly consistent with proxy-data. In agreement with the model results, all available proxies indicate warmer Tortonian temperatures in the high latitudes but obviously the warming of the high latitudes in our model run is much less than indicated by proxy data. According to Wolf and Thiede (1991) there was only sporadic ice rafting in the Upper Miocene North Atlantic. Wolfe (1994) demonstrates that the mean annual temperature of Beringia was about 2–4 °C higher than today whereas the model shows a warming of 1–2 °C only.

Even more serious discrepancies between model temperatures and proxy-data exist for the mid-latitudes of Europe. The model predicts a cooling for the Tortonian mid-latitudes because of a weaker Gulf Stream and ocean heat transport. Terrestrial proxy data, however, clearly indicate that the European continent was warmer and more humid during the Tortonian than today (e.g., Bruch, 1998; Utescher et al.,

2000). This feature, i.e. increased temperature in Europe despite a reduced gulf stream, is not reproduced in our Tortonian model which tends to be too cold in the mid-latitudes and in the high northern parts of Europe and Asia as compared to proxy data (e.g., Wolfe, 1994; Bruch, 1998).

The observed discrepancies between model results and proxy-data may be due to various reasons. First, the prescribed palaeogeography and palaeorography may not be correct. The importance of changes in the orography to the atmospheric circulation was emphasised in many studies (e.g., Ramstein et al., 1997) and our Tortonian orography may be unrealistic in some regions. Furthermore, our model utilised the present-day land–sea distribution which is close but not identical to the Tortonian situation. For instance, in the Tortonian there existed a Paratethys and the Australian continent was further southward of the equator (e.g., Ramstein et al., 1997; Fluteau et al., 1999). The effect of palaeogeography on the climate system has been documented repeatedly (e.g., Upchurch et al., 1998). Barron (1985) demonstrated that the palaeogeographic changes partly contributed to the Cenozoic cooling trend. Fluteau et al. (1999) in their study of the Asian monsoon over the last 30 Ma used a more realistic geography. They varied the size of the Paratethys and shifted the Australia continent further south of the equator. The climatic effect of the Neogene Paratethys is also discussed by Ramstein et al. (1997); they concluded that the shrinking of the Paratethys contributed to the Cenozoic cooling in Central Eurasia and to the increase of monsoonal precipitation. Our modelling results are largely consistent with these previous studies. Hence, the fact that our modelling study is based on the present-day land–sea distribution cannot explain the above-described major discrepancies between our model results and the proxy-data. In this context it should be emphasised again that our study included the effect of an open Central American Isthmus by adjusting the palaeo-flux correction.

The atmospheric CO_2 concentration is another factor which may have caused minor differences between model results and proxy-data. Both the Tortonian and Control run used a concentration of 353 ppm which may not reflect the real Tortonian value. The atmospheric CO_2 concentration during the Miocene was analysed by various authors (e.g., van der Burgh et al., 1993; Pagani et al., 1999) and the results are contentious. Pagani et al. (1999) suggested a Tortonian CO_2-level similar to the pre-industrial one (about 280 ppm). In contrast, van der Burgh et al. (1993) estimated the Tortonian carbon dioxide concentration to range between 380 and 400 ppm. Since a doubling of the CO_2 concentration typically leads to an increase of 2.5–4 °C of the global average temperature (e.g. McGuffie et al., 1999), a change of the CO_2 concentration in our model to the value suggested by van der Burgh et al. (1993) would only induce a slight warming of the model atmosphere. However, considering the uncertainties of reconstructing palaeo-CO_2 concentrations, there is still the possibility that the real Tortonian CO_2 concentration was considerably higher than 400 ppm.

Finally, it should be mentioned that our modelling study uses the modern vegetation distribution. Based on sensitivity studies with the GENESIS model, Dutton and Barron (1996) concluded that a change in the vegetation can lead to a change in the global average temperature of ±1 °C. Later, Dutton and Barron (1997) used an appropriate palaeo-vegetation in a GENESIS modelling study of the Miocene which led to a significant warming and a relatively weak meridional temperature gradient. It should be emphasised, however, that in the analysis of Dutton and Barron (1997) the mixed-layer ocean was not adapted to the Tortonian δ^{18}O-data. Furthermore, Otto-Bliesner and Upchurch (1997) in their study of the Cretaceous observed a warming effect of the vegetation of up to 2.2 °C. Thus, an appropriate reconstruction of the Tortonian vegetation is required in future modelling approaches and should minimise existing discrepancies.

6. Conclusions

Considering both the modelling results for the atmosphere and ocean the following conclusions can be stated:

- The ocean fields modelled with ECHAM/ML for the Late Miocene are in good agreement with oceanic proxy data and with OGCM modelling studies. Our model results document less intense ocean currents–like the Gulf Stream, Kuroshio, Humboldt, and Benguela Current–in the Northern and Southern Hemisphere.
- Thus the proposed method to adapt the flux-correction of a mixed-layer ocean to the palaeo-situation based on oxygen isotope data proved to be reasonable. In addition it was documented that this approach is relatively robust with respect to uncertainties in the interpretation of the oxygen isotope data.

- Regarding the atmosphere and the sea ice, the Tortonian run is mostly in qualitative agreement with proxy-data. For instance, sea ice extent and volume are decreased, the high latitudes show a significant warming, Southern Europe receives more rainfall and the Asian monsoon is reduced. According to the proxies, however, the warming of the high latitudes and the reduction of sea ice was much more intense in the Tortonian than in our simulation. For the Tortonian, some Southern European proxy data (e.g., Southern Spain) also support more arid conditions, which is not consistent with the Standard Tortonian simulation.
- The major differences between our model results and the proxy-data concern the temperature field in the mid-latitudes which in the model are lower than today–caused by the reduced oceanic heat transport–whereas the proxies clearly indicate temperatures above present-day level.
- Despite some minor inconsistencies, the results of the Standard Tortonian run basically agree quite well with proxy data. However, a more detailed (quantitative) comparison of the Tortonian model results with proxy data, which is planned for a separate forthcoming publication (Steppuhn et al., submitted for publication), should clarify how serious the discrepancies really are.
- The observed inconsistencies of our Tortonian run with proxy-data may be due to unrealistic boundary conditions. The above discussion, however, indicates that consideration of the Tortonian vegetation in the model can be expected to significantly improve the results. Obviously, more sensitivity studies regarding the Tortonian boundary conditions are required.

Acknowledgements

The authors would like to thank the Deutsche Forschungsgemeinschaft for their financial support of the special research program ‘SFB275’ at the University of Tübingen. Furthermore, there were some people who basically contributed to our studies. Amongst others, they include: Dr. A.A. Bruch, Dr. M. Gebka, Prof. Dr. C. Hemleben, PD Dr. G. Schmiedl, Dr. D. Uhl. In particular we would like to thank PD Dr. A. Kuhlemann who provided the information about the Tortonian palaeorography.

Simulations with the model ECHAM4/ML were kindly granted by the Max Planck Institute of Meteorology, Hamburg, with special support by Dr. E. Roeckner and Dipl.-Met. U. Schlese.

References

Agustí, J., Meulenkamp, J., Oms, O., 2006. Introduction to the late miocene to early pliocene environment and climate change in the Mediterranean area. Palaeogeography, Palaeoclimatology, Palaeoecology 238, 1–4. doi:10.1016/j.palaeo.2006.03.041.

Attendorn, H.G., Bowen, R.N.C., 1997. Radioactive and Stable Isotope Geology. Chapman and Hall, London. 522 pp.

Barron, E.J., 1985. Explanations of the Tertiary global cooling trend. Palaeogeography, Palaeoclimatology, Palaeoecology 50, 45–61.

Barron, E.J., Peterson, W.H., 1991. The Cenozoic ocean circulation based on ocean general circulation model results. Palaeogeography, Palaeoclimatology, Palaeoecology 83, 1–28.

Berberich, D., 1996. Die planktische Foraminifere Neogloboquadrina Pachyderma (Ehrenberg) im Weddelmeer, Antarktis, vol. 196. Berichte zur Polarforschung. 193 pp.

Bice, K.L., Scotese, C.R., Seidov, D., Barron, E.J., 2000. Quantifying the role of geographic change in Cenozoic ocean heat transport using uncoupled atmosphere and ocean models. Palaeogeography, Palaeoclimatology, Palaeoecology 161, 295–310.

Bigg, G.R., 1999. The Oceans and Climate. Cambridge University Press, Cambridge. 266 pp.

Broecker, W.S., 1989. The salinity contrast between the Atlantic and Pacific Ocean during glacial time. Palaeoceanography 4, 207–212.

Bruch, A.A., 1998. Palynologische Untersuchungen im Oligozän Sloweniens—Paläo-Umwelt und Paläoklima im Ostalpenraum, vol. 18. Tübinger Mikropaläontologische Mitteilungen. 193 pp.

Carissimo, B.C., Oort, A.H., VonderHaar, T.H., 1985. Estimating the meridional energy transports in the atmosphere and ocean. Journal of Physical Oceanography 15, 82–91.

Carrillo, A., Ruti, P.M., Navarra, A., 2000. Storm tracks and zonal mean flow variability: a comparison between observed and simulated data. Climate Dynamics 16, 219–228.

Cohen-Solal, E., Le Treut, H., 1997. Role of the oceanic heat transport in climate dynamics. A sensitivity with an atmospheric general circulation model ocean heat transport GCM sensitivity studies. Tellus 49A, 371–387.

Collins, L.S., Coates, A.G., Berggren, A.G., Aubry, M.P., Zhang, J., 1996. The late Miocene Panama isthmian strait. Geology 24, 687–690.

Craig, H., Gordon, L.I., 1965. Deuterium and oxygen-18 variations in the ocean and the marine atmosphere. In: Stable isotopes in oceanographic studies and palaeotemperatures, Spoleto: 1–122, Pisa, Consiglio Nazionale delle Richerche, Laboratorio di Geologica Nucleare.

Danabasoglu, G., 1998. On the wind-driven circulation of the uncoupled and coupled NCAR climate system ocean model. Journal of Climate 11, 1442–1454.

DKRZ Modellbetreuungsgruppe, 1994. The ECHAM3 Atmospheric General Circulation Model. Technical Report 6, Deutsches Klimarechenzentrum, Hamburg. 182 pp.

DKRZ Modellbetreuungsgruppe, 1997. ECHAM4- Workshop Hamburg, November 25th 1996. Deutsches Klimarechenzentrum, Hamburg.

Dutton, J.F., Barron, E.J., 1996. Genesis sensitivity to changes in past vegetation. Palaeoclimates 1, 325–354.

Dutton, J.F., Barron, E.J., 1997. Miocene to present vegetation changes: A possible piece of the Cenozoic puzzle. Geology 25 (1), 39–41.

Erez, J., Luz, B., 1983. Temperature control of oxygen-isotope fractionation of cultured planktonic foraminifera. Nature 297, 220–222.

Faure, G., 1986. Principles of Isotope Geology, 2nd ed. John Wiley and Sons, New York. 589 pp.

Flower, B.P., Kennett, J.P., 1994. The middle Miocene climatic transition: East Antarctic ice sheet development, deep ocean circulation, and global carbon cycling. Palaeogeography, Palaeoclimatology, Palaeoecology 108, 537–555.

Fluteau, F., Ramstein, G., Besse, J., 1999. Simulating the evolution of the Asian and African monsoons during the past 30 Myr using an atmospheric general circulation model. Journal of Geophysical Research 104, 11995–12018.

Ganachaud, A., Wunsch, C., 2000. Improved estimates of global ocean circulation, heat transport and mixing from hydrographic data. Nature 408, 453–457.

Ganopolski, A., Kubatzki, C., Claussen, M., Brovkin, V., Petoukhov, V., 1998. The influence of vegetation–atmosphere–ocean interaction on climate during the Mid-Holocene. Science 280, 1916–1919.

Ganopolski, A., Rahmstorf, S., Petoukhov, V., Claussen, M., 1998. Simulation of modern and glacial climates with a coupled global model of intermediate complexity. Nature 391, 351–356.

Gleckler, P.J., Randall, D.A., Boer, G., Colman, R., Dix, M., Galin, V., Hefand, M., Kiehl, J., Kitoh, A., Lau, W., Liang, X.Y., Lykossov, V., McAvancey, B., Miyakoda, K., Planton, S., Stern, W., 1995. Cloud-radiative effects on implied oceanic energy transports as simulated by atmospheric general circulation models oceanic heat transport climate modelling GCM. Geophysical Research Letters 22 (7), 791–794.

Harrison, D.E., 1989. On climatological monthly mean wind stress and wind stress curl fields over the world ocean. Journal of Climate 2, 57–70.

Hastenrath, S., 1982. On Meridional Heat Transports in the World Ocean. Journal of Physical Oceanography 12, 922–927.

Haug, G.H., Tiedemann, R., 1998. Effect of the formation of the Isthmus of Panama on Atlantic Ocean thermohaline circulation. Nature 393, 673–676.

Haywood, A.M., Valdes, P.J., Sellwood, B.W., 2000. Global scale palaeoclimate reconstruction of the middle Pliocene climate using the UKMO GCM: initial results. Global and Planetary Change 25, 239–256.

Hellermann, S., Rosenstein, M., 1983. Normal monthly wind stress over the world ocean with error estimates. Journal of Physical Oceanography 13, 1093–1104.

Hemleben, C., Spindler, M., Anderson, O.R., 1989. Modern Planktonic Foraminifera. Springer-Verlag, New York. 363 pp.

Herterich, K., Berger, A., 1993. Modelling the last ice-age cycle with 2-D climate models. Palaeogeography, Palaeoclimatology, Palaeoecology 103, 107–116.

Hsiung, J., 1985. Estimates of global oceanic meridional heat transport. Journal of Physical Oceanography 15, 1405–1413.

Kubatzki, C., Montoya, M., Rahmstorf, S., Ganopolski, A., Claussen, M., 2000. Comparison of the last interglacial climate simulated by a coupled global model of intermediate complexity and AOGCM. Climate Dynamics 16, 799–814.

Kutzbach, J.E., Guetter, P.J., Ruddiman, W.F., Prell, W.L., 1989. Sensitivity of climate to late Cenozoic uplift in southern Asia and the American West. Journal of Geophysical Research 94, 18393–18407.

Latif, M., Neelin, J.D., 1994. El Niño/Southern Oscillation. Technical Report 129, Max-Planck-Institut für Meteorologie, Hamburg. 24 pp.

Leetmaa, A., Bunker, A., 1978. Updated charts of the mean annual wind stress, convergences in the Ekman layers, and Sverdrup transports in the North Atlantic. Journal of Marine Research 36 (2), 311–322.

Lorenz, S., Grieger, B., Helbig, P., Herterich, K., 1996. Investigating the sensitivity of the atmospheric general circulation model ECHAM3 to palaeoclimatic boundary conditions. Geologische Rundschau 85 (3), 513–524.

Maier-Reimer, E., Mikolajewicz, U., Crowley, T., 1990. Ocean general circulation model sensitivity experiment with an open central American isthmus. Palaeoceanography 5 (3), 349–366.

McGuffie, K., Henderson-Sellers, A., Holbrook, N., Kothavalo, Z., Balachova, O., Hoekstra, J., 1999. Assessing simulations of daily temperature and precipitation variability with global climate models for present and enhanced greenhouse climates. International Journal of Climatology 19, 1–26.

Mikolajewicz, U., Crowley, T.J., 1997. Response of a coupled ocean/energy balance model to restricted flow through the central American isthmus. Palaeoceanography 12 (3), 429–441.

Mikolajewicz, U., Maier-Reimer, E., Crowley, T.J., Kim, K.J., 1993. Effect of Drake and Panamanian gateways on the circulation of an ocean model. Palaeoceanography 8 (4), 409–426.

Molnar, P., England, P., Martinod, J., 1993. Mantle Dynamics, uplift of the Tibetan Plateau and the Indian monsoon. Reviews of Geophysics 31 (4), 357–396.

Montoya, M., Crowley, T.J., von Storch, H., 1998. Temperatures at the last interglacial simulated by a coupled ocean–atmosphere climate model. Paleoceanography 13 (2), 170–177.

Niebler, H.S., 1995. Rekonstruktion von Paläo-Umweltparametern anhand von stabilen Isotopen und Faunen-Vergesellschaftungen planktischer Foraminiferen im Südatlantik, vol. 167. Berichte zur Polarforschung. 198 pp.

Nikolaev, S.D., Oskina, N.S., Blyum, N.S., Bubenshchikova, N.V., 1998. Neogene-Quarternary variations of the 'Pole-Equator' temperature gradient of the surface oceanic waters in the North Atlantic and North Pacific. Global and Planetary Change 18, 85–111.

Norris, R.D., Corfield, R.M., Cartlidge, J.E., 1994. Evolutionary ecology of Globorotalia (Globoconella) (planktic foraminifera). Marine Micropalaeontology 23, 121–145.

Otto-Bliesner, B.L., Upchurch Jr., G.R., 1997. Vegetation-induced warming of high latitude regions during the Late Cretaceous period. Nature 385, 804–807.

Pagani, M., Arthur, M.A., Freeman, K.H., 1999. Miocene evolution of atmospheric carbon dioxide. Paleoceanography 14 (3), 273–292.

Pearson, P.N., Ditchfield, P.W., Singano, J., Harcourt-Brown, K.G., Nicholas, C.J., Olsson, R.K., Shackleton, N.J., Hall, M.A., 2001. Warm tropical sea surface temperatures in the Late Cretaceous and Eocene epochs. Nature 413, 481–487.

Prell, W.L., Kutzbach, J.E., 1992. Sensitivity of the Indian monsoon to forcing parameters and implications for its evolution. Nature 360, 647–652.

Ramstein, G., Fluteau, F., Besse, J., Joussaume, S., 1997. Effect of orogeny, plate motion and land–sea distribution on Eurasian climate change over past 30 million years. Nature 386, 788–795.

Roeckner, E., Arpe, K., Bengtsson, L., Brinkop, S., Dümenil, L., Esch, M., Kirk, E., Lunkeit, F., Ponater, M., Rockel, B., Sausen, R., Schlese, U., Schubert, S., Windelband, M., 1992. Simulation of the present-day climate with the ECHAM model: impact of model physics and resolution. Report, vol. 93. Max-Planck-Institut für Meteorologie, Hamburg. 171 pp.

Roeckner, E., Oberhuber, J.M., Bacher, A., Christoph, M., Kirchner, I., 1993. ENSO variability and atmospheric response in a global

coupled atmosphere–ocean GCM. Climate Dynamics 12, 737–754.

Roeckner, E., Arpe, K., Bengtsson, L., Christoph, M., Claussen, M., Dümenil, L., Esch, M., Giorgetta, M., Schlese, U., Schulzweida, U., 1996. The atmospheric general circulation model ECHAM-4: Model description and simulation of present-day climate. Report, vol. 218. Max-Planck-Institut für Meteorologie, Hamburg. 90 pp.

Roemmich, D., Wunsch, C., 1985. Two transatlantic sections: meridional circulation and heat flux in the subtropical North Atlantic Ocean. Deep Sea Research 32, 629–664.

Rohling, E.J., Cooke, S., 1999. Stable oxygen and carbon isotopes in foraminiferal carbonate shells. In: Barun, K., Gupta, S. (Eds.), Modern Foraminifera. Kluwer Academic Publishers, p. 351.

Ruddiman, W.F., Kutzbach, J.E., 1989. Forcing of late Cenozoic northern hemisphere climate by uplift in southern Asia and the American West. Journal of Geophysical Research 94, 18409–18427.

Rye, D.M., Sommer, M.A., 1980. Reconstructing palaeotemperature and palaeosalinity regimes with oxygen isotopes. In: Rhoads, D., Lutz, R. (Eds.), Skeletal Growth of Aquatic Organisms. Plenum Press, New York, p. 750 S.

Savin, S.M., Abel, L., Barrera, E., Hodell, D., Keller, G., Kennett, J.P., Killingley, J., Murphy, M., Vincent, E., 1985. The evolution of Miocene surface and near-surface marine temperatures: oxygen isotopic evidence. Geological Society of America, Memoir 163, 49–73.

Sellwood, B.W., Valdes, P.J., Price, G.D., 2000. Geological evaluation of multiple general circulation model simulations of Late Jurassic palaeoclimate. Palaeogeography, Palaeoclimatology, Palaeoecology 156, 147–160.

Steppuhn, A., Micheels, A., Mosbrugger, V., submitted for publication. The sensitivity of ECHAM4/ML to a double CO_2 scenario for the Late Miocene and the comparison to terrestrial proxy data. Global and Planetary Science.

Thiede, J., Winkler, A., Wolf-Welling, T., Eldholm, O., Myhre, A.M., Baumann, K.-H., Henrich, R., Stein, R., 1998. Late Cenozoic history of the Polar North Atlantic: results from ocean drilling. Quarternary Science 17, 185–208.

Timmermann, A., Latif, M., Grötzner, A., Voss, R., 1999. Modes of climate variability as simulated by a coupled general circulation model: Part I. ENSO-like climate variability and its low-frequency modulation. Climate Dynamics 15, 605–618.

Townsend, T., Hurlburt, H.E., Hogan, P.J., 2000. Modeled Sverdrup flow in the North Atlantic from 11 different wind stress climatologies. Dynamics of Atmospheres and Oceans 32, 373–417.

Trenberth, K.E., Large, W.G., Olson, J.G., 1990. The mean annual cycle on global ocean wind stress. Journal of Physical Oceanography 20, 1742–1760.

Tsuchi, R., 1997. Marine climatic responses to Neogene tectonics of the pacific ocean seaways. Tectonophysics 281, 113.124.

Upchurch Jr., G.R., Otto-Bliesner, B.L., Scotese, C.R., 1998. Vegetation–atmosphere interactions and their role in global warming during the latest Cretaceous. Philosophical Transactions of the Royal Society of London. B 353, 97–112.

Upchurch Jr., G.R., Otto-Bliesner, B.L., Scotese, C.R., 1999. Terrestrial vegetation and its effect on climate during the latest Cretaceous. Geological Society of America, Special Paper 332, 407–426.

Utescher, T., Mosbrugger, V., Ashraf, A.R., 2000. Terrestrial climate evolution in northwest Germany over the last 25 million years. Palaios 15 (5), 430–449.

van der Burgh, J., Visscher, H., Dilcher, D.L., Kürschner, W.M., 1993. Paleoatmospheric Signatures in Neogene Fossil Leaves. Science 260, 1788–1790.

von Storch, H., Zwiers, F.W., 1999. Statistical Analysis in Climate Research. Cambridge University Press, Cambridge. 484 pp.

Wang, J., Wang, Y.J., Liu, Z.C., Li, J.Q., Xi, P., 1999. Cenozoic environmental evolution of the Quaidam Basin and its implications for the uplift of the Tibetan Plateau and the drying of central Asia. Palaeogeography, Palaeoclimatology, Palaeoecology 152, 37–47.

Wolfe, J.A., 1994. An analysis of Neogene climates in Beringia. Palaeogeography, Palaeoclimatology, Palaeoecology 108, 207–216.

Wolf, T.C.W., Thiede, J., 1991. History of terrigenous sedimentation during the past 10 m.y. in the North Atlantic (ODP Legs 104 and 105 and DSDP Leg 81). Marine Geology 101, 83–102.

Woodruff, F., Savin, S.M., 1989. Miocene deepwater oceanography. Palaeoceanography 4, 87–140.

Woodruff, S.D., Lubker, S.J., Wolter, K., Woley, S.J., Elms, J.D., 1993. Comprehensive Ocean–Atmosphere Data Set (COADS) Release 1a: 1980–1992. Earth System Monitor, 4, no.1, September 1993, NOAA.

Wright, J.D., Miller, K.G., 1996. Control of North Atlantic Deep Water circulation by the Greenland–Scotland ridge. Palaeoceanography 11 (2), 157–170.

Zachos, J.C., Stott, L.D., Lohmann, K.C., 1994. Evolution of early Cenozoic marine temperatures. Palaeoceanography 9 (2), 353–387.